Major Project-II

CFD MODELLING OF FLOW THROUGH S - SHAPED DUCT

Submitted in partial fulfillment of the requirement

For the award of the degree of

Master of Technology

In

Thermal Engineering

Submitted By

MD NADIM SHAMS

Roll No. 2K12/THR/15

Under the guidance of

DR. RAJ KUMAR SINGH

Associate Professor

Mechanical Engineering Department

DEPARTMENT OF MECHANICAL, PRODUCTION & INDUSTRIAL AND AUTOMOBILE ENGINEERING

DELHI TECHNOLOGICAL UNIVERSITY, DELHI

2012-2014

DECLARATION

I hereby declare that the work, which is being presented in this dissertation, entitled **" CFD MODELLING OF FLOW THROUGH S-SHAPED DUCT "** towards the partial fulfillment of the requirements for the award of the degree of Master of Technology with specialization in Thermal Engineering, from Delhi Technological University Delhi, is an authentic record of my own work carried out under the supervision of **DR. RAJ KUMAR SINGH** Associate Professor, Department of Mechanical Engineering, at Delhi Technological University, Delhi.

The matter embodied in this dissertation report has not been submitted by me for the award of any other degree.

Md Nadim Shams

2K12/THR/15

Place: Delhi

Date:

This is to certify that the above statement made by the candidate is correct to the best of my knowledge.

DR. RAJ KUMAR SINGH

Associate Professor

Department of Mechanical Engineering

Delhi Technological University

Delhi-110042

CERTIFICATE

It is certified that Md Nadim Shams Roll no. 2K12/THR/15, student of M.Tech Thermal Engineering, Delhi Technological University, has submitted the dissertation titled entitled **" CFD MODELLING OF FLOW THROUGH S-SHAPED DUCT "** under my guidance towards the partial fulfillment of the requirements for the award of the degree of Master of Technology.

He has developed a mathematical computational model of flow through 'S' shaped duct using CFD software. His work is found to be satisfactory and his discipline impeccable during the course of the project. His enthusiasm, attitude towards the project is appreciated.

I wish him success in all his endeavors.

DR. RAJ KUMAR SINGH
Associate Professor
Department of Mechanical Engineering
Delhi Technological University
Delhi-110042

ACKNOWLEDGEMENT

Generally, individuals set aims, but more often than not, their conquest are by the efforts of not just one but many determined people. This complete project could be accomplished because of contribution of a number of people. I take it as a privilege to appreciate and acknowledge the efforts of all those who have, directly or indirectly, helped me achieving my aim.

I take great pride in expressing my unfeigned appreciation and gratitude to my guide, DR. RAJ KUMAR SINGH, Associate Professor, Department of Mechanical Engineering, for his invaluable inspiration, guidance and continuous encouragement throughout this project work.

Md Nadim Shams

2K12/THR/15

ABSTRACT

Flows in S-shaped ducts find applications in aircraft air intakes. This Project report investigates the flow inside an'S' Shaped square Duct. In this report, a computational fluid dynamics (CFD) model of fully developed turbulent flow(k-ϵ model) is implemented with the help of FLUENT software and the variation of pressure along the length of bend with variation in Reynolds number is analysed. The curvatures is investigated at Reynolds numbers Re=4.73x10^4 and 1.47x10^5. A non-dimensional parameter ω, defined as the total pressure loss coefficient is analysed for finding out the total pressure loss in the duct. Cp Data obtained from the simulation of S-shaped ducts show that there is flow separation at the near side wall of the first bend and far side wall of the second bend. At high Reynolds number separation is more dominant near junction of bend as compare to low Reynolds number flow. To improve the flow in S-ducts, vortex generators and tangential blowing as flow control methods are implemented. Vortex generators " locally" mix the high momentum fluid in the free stream with the low momentum fluid near the wall and thus energies the boundary layer to suppress flow separation. Tangential Blowing uses mass addition near the separation point to energies the low momentum fluid close to the wall to overcome the adverse pressure gradient. The two methods suppress flow separation and reduce total pressure loss and to improve flow uniformity at the S-duct exit. These methods shown to be effective in suppressing flow separation and reducing total pressure loss.

TABLE OF CONTENTS

LIST OF FIGURES

LIST OF TABLES

LIST OF SYMBOLS/ABBREVIATIONS

A_{blow} = Cross sectional area of the slot of VG jets

A_{jet} = Cross sectional area of blowing jet

C_P = Pressure coefficient= $\frac{P - P_S}{\frac{1}{2}\rho U_\infty^2}$

C_{PT} = Total pressure coefficient= $\frac{P_T - P_S}{\frac{1}{2}\rho U_\infty^2}$

D = Hydraulic diameter=0.150±0.001 m

D_e = Dean Number = $\sqrt{\frac{D}{2R_C}}.\mathrm{Re}$

g = Acceleration due to gravity= 9.81 m/s^2

h = Height of vortex generators= 0.005 m

L_D = Length of S-duct test section=0.400±0.001 m

L_O = Overall length of S-duct test section=0.800±0.001m

L_S = Length of straight inlet and outlet of S-duct test section=0.200±0.001 m

P = Side wall pressure, N/m^2

ΔP = Radial pressure difference between side walls of S-duct, N/m^2

P_S = Static pressure, N/m^2

P_T = Total Pressure, N/m^2

Q = Flow rate for tangential blowing and vortex generator jets

R_C = Radius of curvature of S-duct

= 0.363 m (Test section 1); 0.290 m (Test Section 2); 0.250 m (Test Section 3)

R_C/D = Curvature ratio of S-duct

= 2.422 (Test Section 1); 1.933 (Test Section 2); 1.667 (Test Section 3)

Re = Reynolds number = 4.73x104, 9.72x104, 1.47x105

S = Cross sectional area of S-duct = 0.152 m2

S_o = Total stream-wise distance for S-shaped duct, m

u, *v*, *w* = Velocity components in *s*, *y* and *z* directions respectively, m/s

u'/U_m = Normalised turbulence intensity

U_m = Mean free stream velocity= 5.00±0.05 m/s, 10.00±0.01 m/s, 15.00±0.15 m/s

α_{vg} = Inclination angle of vortex generator, deg

α_{blow} = Inclination angle of tangential blowing jets, deg

θ = Duct turning angle in deg, 33.4^O (Test Section 1); 43.6^O (Test Section 2); 53.1^O (Test Section 3), 22.5^O (Test Section 4)

ρ = Density of air=1.184±0.012 kg/m3

Ω = Ratio of radial pressure gradient to centrifugal force per unit volume

w = Averaged total pressure loss coefficient between inlet and outlet of S-duct

1. INTRODUCTION

The layout of any practical piping system necessarily includes bends and the accurate prediction of pressure losses, flow rate and pumping requirements demands knowledge of the character of curved duct flows, such wide applications in the industry have forced researchers to acknowledge the importance of study of flow in curved ducts.

Curved duct flows are common in aerospace applications. Many military aircraft have wing root or ventral air intakes and the engine is usually positioned in the Centre of the aircraft's fuselage. Air entering these intake ducts must be turned through two curves (of opposite sign) before reaching the compressor face. Such a configuration results in an S shaped air intake duct and therefore the engine performance becomes a strong function of the uniformity and direction of the inlet flow and these parameters are primarily determined by duct curvature.

This chapter intends to present a review of the flows in curved ducts and S-shaped ducts. Discussion is based on the Flow Separation, mechanism of total pressure loss and duct's exit flow conditions.

1.1 Flows in Curved Ducts and S- Duct

Flows in a bend are influenced predominantly by two related forces because of the Centre-line curvature, the forces being centrifugal force and the radial pressure gradient that exist between outside and inside walls of the curved duct. A helical secondary flow is present in the duct bend . The faster moving fluid near the axis of the duct travels at the highest velocity and is therefore subjected to a larger centrifugal force than the slower moving fluid in the neighborhood of the duct walls. This results in the superposition of a transverse (or radial) motion onto the primary axial flow, in which the fluid in the central region of the duct moves away from the Centre of curvature and towards the outer wall of the bend. As this core fluid approaches the outside wall of the bend, it encounters an adverse pressure gradient and begins to slow down. This energy deficient fluid approaching the outside wall is unable to overcome the adverse pressure gradient, and instead moves around the walls towards the low static pressure region on the inside

of the bend. Two cells of counter rotating secondary flow at the end of the first bend are set up due to movement of low energy fluid towards inside of the bend combined with the deflection of the high velocity core region towards outside of the bend. Thus, for ducts of symmetrical cross section with respect to the plane of the curvature, a secondary flow exists which consists of a pair of helical vortices. The flow structure described above is generally true for curved duct flows and is termed the "two vortex secondary flow" structure in literature. It may be noted that as the flow velocity increases, additional vortical flow structures appear which show a strong dependence on Reynolds number (Re), curvature radius ratio (D/2Rc where D and R_c are the hydraulic diameter and radius of curvature respectively). To account for the effects of the first two parameters, a non-dimensional number, the Dean number (De), is usually used. It is defined as, $\sqrt{\frac{D}{2R_C}}.\mathrm{Re}$

Another facet of the study of flow in S-duct is flow control because these ducts find practical application as aircraft air-intake ducts. The trend in modern fighter aircraft is to have a short and highly curved S-shaped intake duct. The short length reduces the structural weight of the aircraft and increases the internal space packaging efficiency. However, the shortening of the duct results in a highly curved duct profile while still maintaining the correct offset of the engine fan face (housed in the fuselage) and the intake entrance face (at the exterior of the fuselage). Although the short intake duct is highly desirable for its compactness and weight reduction, it is aerodynamically inefficient, as it is highly susceptible to massive flow separation. In addition, the flow is coupled with bulk swirl with the presence of stream-wise vortices. These flow features lead to total pressure losses in the duct, flow distortion at the duct exit and hence flow non-uniformity at the engine fan face.

The improvements in performance of S-shaped ducts are thus a reduction in flow distortion at the duct exits, maximizing the flow rate and hence minimizing the total pressure losses and elimination of flow separation if it is present. These requirements involve flow control devices like vortex generators, blowing techniques and vortex generator jets to suppress flow separation, and fences to attenuate swirl.

2. LITERATURE REVIEW

2.1 FLOW IN S-SHAPED DUCTS

The internal flows in curved S-shaped ducts are often found in various aerodynamics and fluid mechanics applications, where a combination of bends is employed to re-direct the flow. A good example is an aircraft jet engine intake. Similar to the flow in a simple curved duct, flows in S-ducts are influenced predominately by two related forces, namely, the centrifugal forces and the radial pressure gradients that exist between the outside and inside walls of the curved duct resulting in the formation of secondary flow. The description in the previous sections for swirling flow in a single bend also occurs in the first bend of an S-duct. Hence, a pair of helical vertical flow exists in the first bend of the S-duct. Additional complex flow structures form when the flow enters the second bend of opposite curvature. In the second bend, the swirl that developed initially in the first bend of an S-duct is attenuated and reversed in the second bend due to the opposite curvature and the reversed radial pressure gradient. Since an S-duct consists of bends of opposite curvature and the radial pressure gradient changes sign along the S-duct, the side wall pressure distribution is sinusoidal-like in shape.

2.2 Literature Review

Kitchen and Bowyer et al (1989)investigated At the inlet of the duct, the high and low pressure side walls are respectively at the outer wall and inner wall of the first bend. The high and low pressure side changes in the second bend to reflect the change in duct curvature. The observation on swirl development in S-duct is generally true for both circular and non-circular geometry.

Bansod and Bradshaw **(1972)** ***and Taylor et al.*** **(1984)** (both for circular cross-sectioned S-duct) and ***Sugiyama et al.*** **(1997) and** ***Taylor et al.*** **(1982a)** (both for square cross sectioned S-duct) drew similarities between them. Firstly, it was noted that the swirl flow in the second bend still retains a distinctive symmetrical, two cell swirl configuration at the S-duct exit. Secondly, core flow (or fluid with high flow velocity) in the S-duct migrates towards the outside wall of the first bend and exits

near the inside wall of the second bend. Lastly, large scale, vertical structures exist along the outside wall of the second bend in both the circular and square cross-sectioned S-ducts. This finding is consistent with many other works.

Anderson et al. **(1982) and** ***Cheng and Shi*** **(1991)** (for square cross-sectioned S-ducts) In particular, the development of longitudinal vortices near the wall is accompanied by the rapid thickening of the boundary layer at the outside wall of the second bend. taken from Bansod and Bradshaw (1972) on circular S-shaped duct, shows the total pressure distribution on the S-duct exit and the thickened boundary layer along the outside wall of the second bend. The core flow exists close to the inside wall of the second bend. Bansod and Bradshaw (1972) pointed out that since a favorable longitudinal pressure gradient exists on the outside wall of the second bend, the flow near this wall is accelerating and hence these longitudinal vortices could undergo " vortex stretching" , thus intensifying vorticity. This causes the boundary layer near that wall to thicken rapidly due to enhanced entrainment and accumulate into a region of low momentum fluid. Another variant in S-duct flows is the S-shaped diffuser which can be found in many applications. In addition to the combined effects of centrifugal forces and radial pressure gradient in S-duct flows, flow separation is another important factor that influences the flow structure in an S-duct diffuser. Due to the increasing cross sectional area, a stream-wise adverse pressure gradient is also present. The combined effects may result in increased flow non-uniformity and total pressure loss at the duct exit as compared to a uniformed cross sectioned S-duct. In a circular cross sectioned S-duct diffuser, flow separation results in a comparatively large pair of contra-rotating stream-wise vortices, which occupy about a third to a half of the S-duct exit area. Such problems were investigated by Whitelaw and Yu (1993a, b) and Yu and Goldsmith (1994), Anderson et al. (1994) for circular cross sectioned diffusers.

Rojas et al**. (1983*), Sullerey and Pradeep*** **(2003), and Pradeep and Sullerey (2004**). The flow in S-duct diffusers of rectangular or square cross section were studied Among these works on constant cross sectioned S-duct or diffusers, the effects of inlet boundary layer play an important role in the swirl development.

Anderson et al. (1982) (for constant square S-duct), Rojas et al. (1983) (for square S-duct diffuser) and **Whitelaw and Yu (1993a)** (for circular S-duct diffuser),), investigated the effects of boundary layer thicknesses in their respective studies. Similar to the case of a single 90^0 bend, flows with a thicker inlet boundary layer result in a larger magnitude swirl generated in the first bend. The difference in swirl magnitude can be 0.22Um and 0.15Um for the thick and thin boundary cases noted by Anderson et al. (1982). Rojas et al. (1983) and Whitelaw and Yu (1993a) quoted respectively 0.4Umversus 0.15Um and 0.16Um versus 0.12Um for the corresponding thick and thin boundary layer cases. However, the details in flow topology within the second bend are dependent on whether flow separation is present. For the work of Anderson et al. (1982) and Rojas et al. (1983) where flow separation is not present, increasing the inlet boundary layer thickness led to a corresponding increase in boundary layer development along the outer wall of the second bend. However, for Whitelaw and Yu (1993a) where flow separation is present, they found that an increase in inlet boundary layer thickness led to a corresponding decrease in boundary layer thickness along the outer wall of the second bend. Whitelaw and Yu (1993a) also found that increasing inlet boundary layer led to a reduction in separation region in their S-duct study and argued that the earlier reattachment of separated flow for the thick inlet boundary layer case led to a corresponding decrease in outlet boundary layer along the outer wall of the second bend. Their LDA measurements show this very clearly. The above review has concentrated mainly on S-duct with limited turning angle at relatively high Re (or De) where Dean vortices are not present. It is of interest to study flows within the critical Dean number range and where the turning angle in the first bend of the S-duct is large enough to initiate the formation of Dean vortex and investigate the flow structure in the second bend of opposite curvature.

Cheng and Shi et al (1991) studied such flows using flow visualization only and in a Dean number range of 25 to 350. The square cross sectioned S-duct bend has curvature ratio (Rc/D) of 2.5, with turning angle of 225^0 for both bends. Their results show that Dean vortices formed at De = 101, 151, 201 and 252 and at a turning angle of about 180^0 in the first bend. These vortices continue to grow until 225^0 within the first bend and with increasing asymmetric structure for the higher De 201,

while the vortices stay relatively symmetric for lower De of 101 and 151. the formation of a pair of Dean vortices on the outer wall of the first bend at De = 151 at 225^0 Upon entering the second bend, the curvature of the outer and inner wall changes and the direction of the centrifugal force also changes accordingly. At 45^0 into the second bend, Cheng and Shi (1991) noted that there still exist some remnants of the Dean vortices on the inner wall of the second bend that was generated on the outer wall of the first bend. These occur at low De = 151 and 200. These decaying Dean vortices disappear as they are suppressed by secondary flow generated in the second bend. A new set of Dean vortices starts to appear on the outer wall of the second bend at about 135^0 into the second bend and they continue to grow downstream. Flows at higher De > 200 seem to display complex and asymmetrical structures in the second bend. Cheng and Shi (1991) can identify 6 vortices including the dominating Dean vortex at De = 354.

Another facet of the study of flow in S-duct is flow control because these ducts find practical application as aircraft air-intake ducts. The trend in modern fighter aircraft is to have a short and highly curved S-shaped intake duct. The short length reduces the structural weight of the aircraft and increases the internal space packaging efficiency. However, the shortening of the duct results in a highly curved duct profile while still maintaining the correct offset of the engine fan face (housed in the fuselage) and the intake entrance face (at the exterior of the fuselage). Although the short intake duct is highly desirable for its compactness and weight reduction, it is aerodynamically inefficient, as it is highly susceptible to massive flow separation. In addition, the flow is coupled with bulk swirl with the presence of stream-wise vortices. These flow features lead to total pressure losses in the duct, flow distortion at the duct exit and hence flow non-uniformity at the engine fan face.

The improvements in performance of S-shaped ducts are thus a reduction in flow distortion at the duct exits, maximizing the flow rate and hence minimizing the total pressure losses and elimination of flow separation if it is present. These requirements involve flow control devices like vortex generators, blowing techniques and vortex generator jets to suppress flow separation, and fences to attenuate swirl.

Gad-el Hak and Bushnell (1991) and Lin (2002).Separation flow control is discussed . These flow control devices are placed on the side walls of the S-duct and slightly upstream of the separation point. Vortex generators " locally" mix the high momentum fluid in the free stream with the low momentum fluid near the wall and thus energize the boundary layer to suppress flow separation.

Vakili et al. (1985), Reichert and Wendt(1996) and Anderson and Gibb (1998) used vortex generators for separation control in circular cross-sectioned S-shaped diffuser

Sullerey and Pradeep (2002) and Sullerey et al. (2002)used vortex generators in a rectangular cross sectioned S-shaped diffuser. Blowing and vortex generator jets use mass addition near the separation point to energise the low momentum fluid close to the wall to overcome the adverse pressure gradient. The former method has the added flexibility of altering the blowing direction.

M. Norouzia, M.H. Kayhani, C. Shu, M.R.H. Nobari et al. (2010) investigates the inertial and creeping flow of a second-order fluid in a curved duct with a square cross-section. Numerical modeling is employed to analyze fluid flow, and the governing equations are discretized using the finite difference method on a staggered mesh. The marker-and-cell method is employed to allocate the parameters on the staggered mesh, and static pressure is calculated using the artificial compressibility approach. The effect of centrifugal force due to the curvature of the duct and the opposing effects of the first and second normal stress difference on the flow field are investigated. In addition, the order-of-magnitude technique is used to derive the force balance relations for the core region of flow. Based on these relations, the performance mechanism of centrifugal force and normal stress differences on the generation of secondary flows is considered.

Xiaoyun Wu, Sangding Lai, Kyoji Yamamoto, Shinichiro Yanase et al (2011) investigated the vortex patterns of the secondary flow in a curved duct of square cross-section are numerically. The flow is driven by the axial pressure gradient as well as the walls rotation of the duct except the outer wall around the center of curvature. When the rotation is in the same direction as the negative pressure gradient, the secondary flow shows complicated multiple

patterns, which consists of two-vortex, four-vortex, eight-vortex or even non-symmetric secondary flow pattern.

Tilak T. Chandratilleke, NimaNadim, Ramesh Narayanaswamy et al (2012) numerical investigation for examining the secondary vortex motion and associated heat transfer process in fluid flow through curved passages. Overcoming current modelling limitations, the study formulates an improved simulation model based on 3-dimensional vortex structures for describing secondary flow and its thermal characteristics. For developing laminar fluid flow through curved rectangular ducts, the analysis performs a detailed parametric study involving the contours of helicity and outer duct wall pressure gradient for a range of flow rates, duct aspect ratios, duct flow curvatures and external wall heat fluxes. The flow conditions leading to hydrodynamic instability and Dean vortex generation in curved passages are carefully analyzed, identifying the flow and geometrical parametric influences. Active interaction of buoyancy force on fluid motion arising from wall heating is considered where aspects of boundary layer separation is used in recognizing thermal enhancement due to secondary flow.

In the light of the exhaustive literature review, it was observed that a good deal of research work has been carried out in the field of experimental analysis of flow and the incurring losses in bends and curvatures. Such types of experimental studies are expensive and time consuming. Besides, the cumulative error margins are also not very satisfactory. Numerical simulation presents a very similar application in such type of situations.

In the view of the above facts, the present research work focuses on numerical simulation of flow across bends using computational fluid dynamics tool.

2.3 Problem Statement

A survey of the current literature reveals that information on the flow in a constant square cross-sectioned S-shaped duct is lacking, especially flow data for S-ducts of large curvature (or sharper bend) and at higher Re. This is the main motivation of the present investigation. The objective is,

To study the Flow separation, total pressure loss at Re=4.73x10^4 and1.47x10^5 in S- ducts with flow control techniques vortex generator and Tangential blowing.

In the current literature, flow in square cross sectioned S-duct of lower curvature were reported by Taylor et al. (1982a), Anderson et al.(1982) and Sugiyama et al.(1997) (in Japanese) and their S-duct geometry had a curvature ratio RC/D = 7, duct turning angle of =22.5 ^{O}, and their investigation was conducted at Re = 750 and $4.0x10^4$. The present work was conducted at higher Re = $4.73x10^4$ and $1.47x10^5$ and with square cross-sectioned, S shaped ducts with sharper bends and larger turning angle.

3. CFD MODELLING

Computational Fluid Dynamics (CFD) can be described as the use of computers to produce information about the ways in which fluids flow in given situations. CFD embraces a variety of technologies including mathematics, computer science, engineering and physics, and these disciplines have to be brought together to provide the means of modeling fluid flows. Such modeling is used in many fields of science and engineering but, if it is to be useful, the results that it yields must be a realistic simulation of a fluid in motion.

3.1 Why Use CFD for analysis:

- CFD can be used to:
    - Improve understanding of how fluid flows under various conditions.
    - Evaluate the flow or new technological performance.
    - Provide conceptual designs.
    - Identify potential operational problems.
    - Guide experiments.
- CFD is more cost-effective than physical testing
- CFD provides more complete information than testing

CFD does NOT make decisions for engineers, but does help them be more informed

FLUENT is a state-of-the-art CFD computer program for modeling fluid flow and heat transfer in complex geometries. FLUENT is a finite volume analysis program for solving fluid flow and conjugate heat transfer problems. The fluid flow problem is defined by the laws of conservation of mass, momentum, and energy. These laws are expressed in terms of partial differential equations which are discretized with a finite volume based technique.

Assumptions about the fluid and the analysis made are:

- There is only one phase.
- The user must determine:
    - If the problem is laminar (default) or turbulent
    - If the incompressible (default) or the compressible algorithm must be invoked

The governing equations solved by FLUENT are the Navier-Stokes equations combined with the continuity equation, the thermal transport equation, and constitutive property relationships.

Continuity Equation

$$\frac{\partial p}{\partial t}+\frac{\partial}{\partial x}\left(\rho v_x\right)+\frac{\partial}{\partial r}\left(\rho v_r\right)=S_m$$

Navier Stokes Equation

$$\frac{\partial}{\partial t}\left(\rho\vec{v}\right)+\nabla.\left(\rho\vec{v}\vec{v}\right)=-\nabla p+\nabla.\left(\bar{\bar{\tau}}\right)+\rho\vec{g}+\vec{F}$$

3.2 Program Capabilities

The FLUENT solver has the following modeling capabilities:

- 2D planar, 2D axisymmetric, 2D axisymmetric with swirl (rotationally symmetric), and 3D flows
- Quadrilateral, triangular, hexahedral (brick), tetrahedral, prism (wedge), pyramid, polyhedral, and mixed element meshes
- Steady-state or transient flows
- Incompressible or compressible flows, including all speed regimes (low subsonic, transonic, supersonic, and hypersonic flows)
- Inviscid, laminar, and turbulent flows
- Newtonian or non-Newtonian flows
- Heat transfer, including forced, natural, and mixed convection, conjugate (solid/fluid) heat transfer, and radiation
- Chemical species mixing and reaction, including homogeneous and heterogeneous combustion models and surface deposition/reaction models
- Free surface and multiphase models for gas-liquid, gas-solid, and liquid-solid flows
- Lagrangian trajectory calculation for dispersed phase (particles, droplets, bubbles), including coupling with continuous phase and spray modeling
- Cavitation model
- Phase change model for melting/solidification applications
- Porous media with non-isotropic permeability, inertial resistance, solid heat conduction, and porous-face pressure jump conditions

- Lumped parameter models for fans, pumps, radiators, and heat exchangers
- Acoustic models for predicting flow-induced noise
- Inertial (stationary) or non-inertial (rotating or accelerating) reference frames
- Multiple reference frame (MRF) and sliding mesh options for modeling multiple moving frames
- Mixing-plane model for modeling rotor-stator interactions, torque converters, and similar turbo-machinery applications with options for mass conservation and swirl conservation
- Volumetric sources of mass, momentum, heat, and chemical species

FLUENT is ideally suited for incompressible and compressible fluid-flow simulations in complex geometries.

3.3 Planning CFD Analysis

The following consideration should be taken while planning CFD analysis:

3.3.1 Definition of the Modeling Goals:

What specific results are required from the CFD model and how will they be used? What degree of accuracy is required from the model?

3.3.2 Grid Generation and its Independence:

What type of element will be used? What size of the mesh should be kept so as to optimize between accuracy and time and resources being consumed?

3.3.3 Choice of the Computational Model:

How will you isolate a piece of the complete physical system to be modeled? Where will the computational domain begin and end? What boundary conditions will be used at the boundaries of the model? Can the problem be modeled in two dimensions or is a three-dimensional model required? What type of grid topology is best suited for this problem?

3.3.4 Choice of Physical Models:

Is the flow inviscid, laminar, or turbulent? Is the flow unsteady or steady? Is heat transfer important? Will you treat the fluid as incompressible or compressible? Are there other physical models that should be applied?

3.3.5 Determination of the Solution Procedure:

Can the problem be solved simply, using the default solver formulation and solution parameters?

Can convergence be accelerated with a more judicious solution procedure? Will the problem fit within the memory constraints of your computer, including the use of multigrain? How long will the problem take to converge on your computer?

Careful consideration of these issues before beginning CFD analysis will contribute significantly to the success of modeling effort.

3.4 Discretization of partial equations

The governing equations are converted into algebraic equations with the help of the finite volume technique that can be solved numerically. This control volume technique consists of integrating the governing equations about each control volume, yielding discrete equations that conserve each quantity on a control-volume basis.

Discretization of the governing equations can be illustrated most easily by considering the steady-state conservation equation for transport of a scalar quantity φ. This is demonstrated by the following equation written in integral form for an arbitrary control volume V as follows:

$$\int \rho\phi\vec{v}.d\vec{A} = \int \Gamma_\phi \nabla\phi.d\vec{A} + \int_V S_\phi dV$$

where

ρ = density

v = velocity vector A = surface area vector

Γ_φ = diffusion co-efficient for φ

φ = gradient of φ

S_φ = source of φ per unit volume

Above equation is applied to each control volume, or cell, in the computational domain. Discretization of Equation on a given cell yields

$$\sum_f^{N_{faces}} \rho_f v_f \phi_f .\vec{A}_f = \sum_f^{N_{faces}} \Gamma_\phi (\nabla\phi)_n .\vec{A}_f + S_\phi V$$

Where

N_{faces} = number of faces enclosing cell

φf = value of φ convected through face f

$\rho_f v_f A_f$ = mass flux through the face

A_f = area of face f,

$(\nabla \varphi)_n$ = magnitude of $\nabla \varphi$ normal to face

V = cell volume

The equations take the same general form as the one given above and apply readily to multi-dimensional, unstructured meshes composed of arbitrary polyhedral, the discrete values of the scalar φ at the cell centers. However, face values φ_f is required for the convection terms in Equation and must be interpolated from the cell center values. This is accomplished using an upwind scheme.

Up winding means that the face value φf is derived from quantities in the cell upstream, or "upwind," relative to the direction of the normal velocity v_n

3.5 Convergence Criteria

Finally, one needs to set the convergence criteria for a iterative method. Deciding when to stop the iterative process is very important, from both the efficiency and accuracy point of view. A numerical is said to be convergent if the solution of the discretized equations tend to exact the solution of the differential as the grid spacing tends to be zero. The convergence criterion of 10^{-6} for all variables is taken for all the iterations.

3.6 Simulation Procedure

(STEP 1) Modeling (In Solid works):

- S-DUCT geometry is created
- Stabilizing length equal to D=.15m was attached at inlet.
- The model has been meshed with quadratic-mesh. Fine meshing with spacing 0.07 was done and mesh elements range from 12000 – 75000 elements.
- Boundary conditions taken were for velocity at inlet, pressure at outlet and wall type for S-duct.
- Fluid was specified as air for the continuum type and the mesh was exported to Fluent for post processing.

(STEP 2) Post Processing (In Fluent):

- Grid was checked and scaled.

- 3D axisymmetric solver and segregated solution method was chosen.
- Air was chosen as the fluid for flow, and its properties were selected.
- K-ε RNG models is selected.
- At air inlet section, the inlet velocity of 5 m/s with different swirl intensity was specified.
- Turbulence intensity of 5% based on inlet flow diameter was specified. At the exit section, the pressure was specified being equal to atmospheric pressure.
- Second order upwind scheme was selected to solve continuity and momentum equations.
- Convergence criteria of 10^{-6} were taken.
- Solution was initialized at inlet and made to iterate until it converges.

Once solution is converged, various data for pressure and velocity were obtained and graphs were plotted.

INPUT PARAMETER:

Parameter	**Turbulent flow**
Area of duct (m^2)	0.225
Length of S bend (m)	3.75
Flowing Fluid	Air
Temperature (K)	283
Density of fluid (Kg/m^3)	1.240722
Viscosity of fluid (kg/ms)	176.10e-07
Reynolds number	$4.73x10^4$ & $1.47x10^5$
Outside Pressure (atm)	1
Flow Model	K-ε model(RNG)
Material of S-bend	Steel

3.7.FLOW FIELD NUMERICAL MODELLING

The present study involves various models and basic laws of fluid mechanics to attain the results. FLUENT provides comprehensive modeling capabilities for a wide range of incompressible laminar and turbulent fluid problems. In FLUENT, a broad range of mathematical models for transport phenomena (like heat transfer swirl and chemical reactions) is combined with the ability to model complex geometries. The range of problems that can be

addressed is very wide. The turbulence models provided have broad range of applicability without the need for fine tuning to a specific application.

3.7.1 TURBULENCE MODELLING

Turbulent flows are characterized by fluctuating velocity fields. These fluctuations mix with transported quantities such as momentum, energy, and species concentration, and cause the transported quantities to fluctuate as well. Since these fluctuations can be of small scale and high frequency, they are too computationally expensive to simulate directly in practical engineering calculations. Instead, the instantaneous (exact) governing equations can be time-averaged, ensemble-averaged, or otherwise manipulated to remove the small scales, resulting in a modified set of equations that are computationally less expensive to solve. However, the modified equations contain additional unknown variables, and turbulence models are needed to determine these variables in terms of known quantities.

3.7.2 Choosing a Turbulence Model

It is an unfortunate fact that no single turbulence model is universally accepted as being superior for all classes of problems. The choice of turbulence model will depend on considerations such as the physics encompassed in the flow, the established practice for a specific class of problem, the level of accuracy required, the available computational resources, and the amount of time available for the simulation. To make the most appropriate choice of model for your application, one needs to understand the capabilities and limitations of the various options. The purpose of this section is to give an overview of issues related to the turbulence models provided in FLUENT. The computational effort and cost in terms of CPU time and memory of the individual models is discussed. While it is impossible to state categorically which model is best for a specific application, general guidelines are presented to help you choose the appropriate turbulence model for the flow you want to model.

3.7.3 FLUENT provides the following choices of turbulence models:

- Spalart-Allmaras model
- k- ε models
    - Standard k- ε model

- Renormalization-group (RNG) k- ε model
- Realizable k- ε model

- k- ω models
  - Standard k- ω model
  - Shear-stress transport (SST) k- ω model
- Reynolds stress model (RSM)
- Large eddy simulation (LES) model

3.8 The Standard, RNG, and Realizable k- ε Models

All three models have similar forms, with transport equations for k and ε. The major differences in the models are as follows:

- the method of calculating turbulent viscosity
- the turbulent Prandtl numbers governing the turbulent diffusion of k and ε
- the generation and destruction terms in the ε equation

The transport equations, methods of calculating turbulent viscosity, and model constants are presented separately for each model.

3.8.1 The Standard k-ε Model

The simplest “complete models" of turbulence are two-equation models in which the solution of two separate transport equations allows the turbulent velocity and length scales to be independently determined. The standard k- ε model in FLUENT falls within this class of turbulence model and has become the workhorse of practical engineering flow calculations in the time since it was proposed by Launder and Spalding. Robustness, economy, and reasonable accuracy for a wide range of turbulent flows explain its popularity in industrial flow and heat transfer simulations. It is a semi-empirical model, and the derivation of the model equations relies on phenomenological considerations and empiricism.

The standard k- ε model is a semi-empirical model based on model transport equations for the turbulence kinetic energy (k) and its dissipation rate (ε). The model transport equation for k is derived from the exact equation, while the model transport equation for ε was obtained using physical reasoning and bears little resemblance to its mathematically exact counterpart.

For k- ε model, it was assumed that the flow is fully turbulent, and the effects of molecular viscosity are negligible, therefore valid only for fully turbulent flows.

3.8.2 The RNG k-ε Model

The RNG-based k-ε turbulence model is derived from the instantaneous Navier-Stokes equations, using a mathematical technique called "renormalization group" (RNG) methods. It is similar in form to the standard k-ε model, but includes the following refinements:

- The RNG model has an additional term in its ε equation that significantly improves the accuracy for rapidly strained flows.
- The effect of swirl on turbulence is included in the RNG model, enhancing accuracy for swirling flows.
- The RNG theory provides an analytical formula for turbulent Prandtl numbers, while the standard k-ε model uses user-specified, constant values.
- While the standard k-ε model is a high-Reynolds-number model, the RNG theory provides an analytically-derived differential formula for effective viscosity that accounts for low-Reynolds-number effects. Effective use of this feature does, however, depend on an appropriate treatment of the near-wall region.

These features make the RNG k-ε model more accurate and reliable for a wider class of flows than the standard k-ε model.

3.8.4 The Realizable k-ε Model

The realizable k-ε model is a relatively recent development and differs from the standard k-ε model in two important ways:

- The realizable k-ε model contains a new formulation for the turbulent viscosity.
- A new transport equation for the dissipation rate, ε, has been derived from an exact equation for the transport of the mean-square vorticity fluctuation.

The term "realizable" means that the model satisfies certain mathematical constraints on the Reynolds stresses, consistent with the physics of turbulent flows. Neither the standard k-ε model nor the RNG k- ε model is realizable. An immediate benefit of the realizable k-ε model is that it more accurately predicts the spreading rate of both planar and round jets. It is also likely to

provide superior performance for flows involving rotation, boundary layers under strong adverse pressure gradients, separation, and recirculation. Since the model is still relatively new, it is not clear in exactly which instances the realizable k-ε model consistently outperforms the RNG model. One limitation of the realizable k-ε model is that it produces non-physical turbulent viscosities in situations when the computational domain contains both rotating and stationary fluid zones (e.g., multiple reference frames, rotating sliding meshes). This is due to the fact that the realizable k- ε model includes the effects of mean rotation in the definition of the turbulent viscosity**.** This extra rotation effect has been tested on single rotating reference frame systems and showed superior behavior over the standard k-ε model.

3.9 FLUENT Applications

FLUENT has been applied to a variety of applications from a wide range of industries.

- **AUTOMOTIVE**
  - Study of air flow over vehicles
  - Passenger compartment flow
  - Fluid flow, conjugate heat transfer analysis of engine exhaust manifolds and water jackets - Flow through radiator passages
  - Flow analysis through various valve configurations
  - Multi-Component fuel spray simulation
  - IC engine simulation
  - innovative intake port design
  - high-speed ground vehicle aerodynamics
- **AEROSPACE**
  - External flow over various wing configurations
  - Internal flow analyses of nozzles and ducts
  - Fluid flow, heat transfer analysis of aircraft passenger compartments
  - Compressible flow analysis with shock/boundary layer interaction
  - Thermal analyses
- **ELECTRONICS**
  - Electronic cooling in a computer terminal
  - Conjugate heat transfer analysis of IC package
  - Heat transfer analysis of electronic fin array

- Heat transfer analysis of a simulated card cage
- Disk flow

- **POWER**
  - Thermally stratified turbulent pipe flow
  - Pressurized thermal shock
  - Natural convection cooling
  - Fluid bed reactor analysis
  - Valve analysis
- **HVAC**
  - Flow inside buildings
  - Flow in ducts
  - Flow in pipes
  - Flow through coolant passages
  - Heat exchanger analysis
- **TURBO MACHINERY**
  - Torque converter flow analysis
  - Flow through vaned and vane-less diffusers
  - Labyrinth seal flow
  - Blade cooling analysis
  - Flow in pump, compressor, turbine, impeller passages
  - Pulse turbo-charging simulation

4. RESULTS AND DISCUSSION

The optimum aerodynamic performance of S-shaped ducts (or aircraft air-intake ducts) demands that a relatively uniform flow with a smallest possible pressure loss. These requirements naturally lead one to consider the use of traditional flow control devices like vortex generators, blowing jets. Passive devices like vortex generators placed on the side wall eliminate flow separation if it is present. They "locally" mix the high-momentum fluid in the free stream with low-momentum fluid near the wall and thus suppress flow separation. In contrast to the passive means of flow control, blowing jets and vortex generator jets are active flow control devices for flow separation control, whereby mass addition near the separation point energizes the low momentum fluid close to the wall to overcome the adverse pressure gradient.

To study the effects of flow control in square cross sectioned S-duct, two different flow control methods were studied, namely, vortex generator and tangential Blowing . In this Chapter, the relative merits of vortex generators and tangential blowing on the flow in a square cross sectioned S-duct. Suppression of flow separation, reduction of total pressure loss, and flow uniformity at duct exit are the chosen criteria.

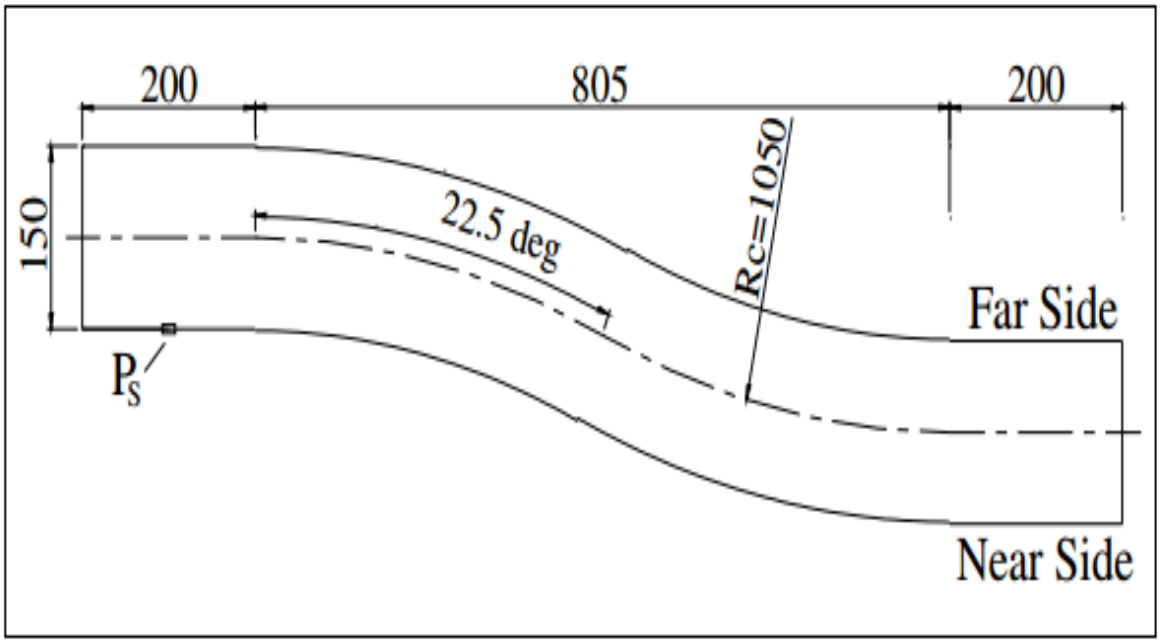

Fig: 1 S-duct configuration [13]

Investigation of (S-duct Fig: 1) has been carried out with help of FLUENT, a CFD tool to simulate the Effect of pressure is studied. The present work is conducted at higher Re=4.73x10^4

and $1.47x10^5$ and with square cross-sectioned, S- shaped ducts with sharper bends and larger turning angle. The geometry is made in solid works and imported on Ansys software for analysis. After analysis on FLUENT following graphs are plotted.

Case 1: Study of 3D S-Shaped Duct:

Mesh Independency Study:

The grid independency is studied for the k-ε model employing four size of grid to examine the sensitivity of grid. As we get result in the third column that is fine mesh size is independent of grid that's the optimum grid.

Table: 1 Grid independency chart

Mesh size	Maximum cell squish	Maximum aspect ratio	Pressure and static pressure(min and maximum)	Pressure and pressure coefficient
coarse	5.05561×10^{-2}	2.03094	-1.37609, 3.683053	-2.246697, 6.013155
medium	6.5253×10^{-2}	2.16342	-1.553137, 3.96047	-2.535753, 6.466074
fine	9.28082×10^{-2}	2.18632	-1.585209, 4.26690	-2.5881, 6.966368
Mesh with sizing	9.28082×10^{-2}	2018632	-1.585209, 4.26690	-2.5881, 6.966368

Graphs of Static Pressure contours

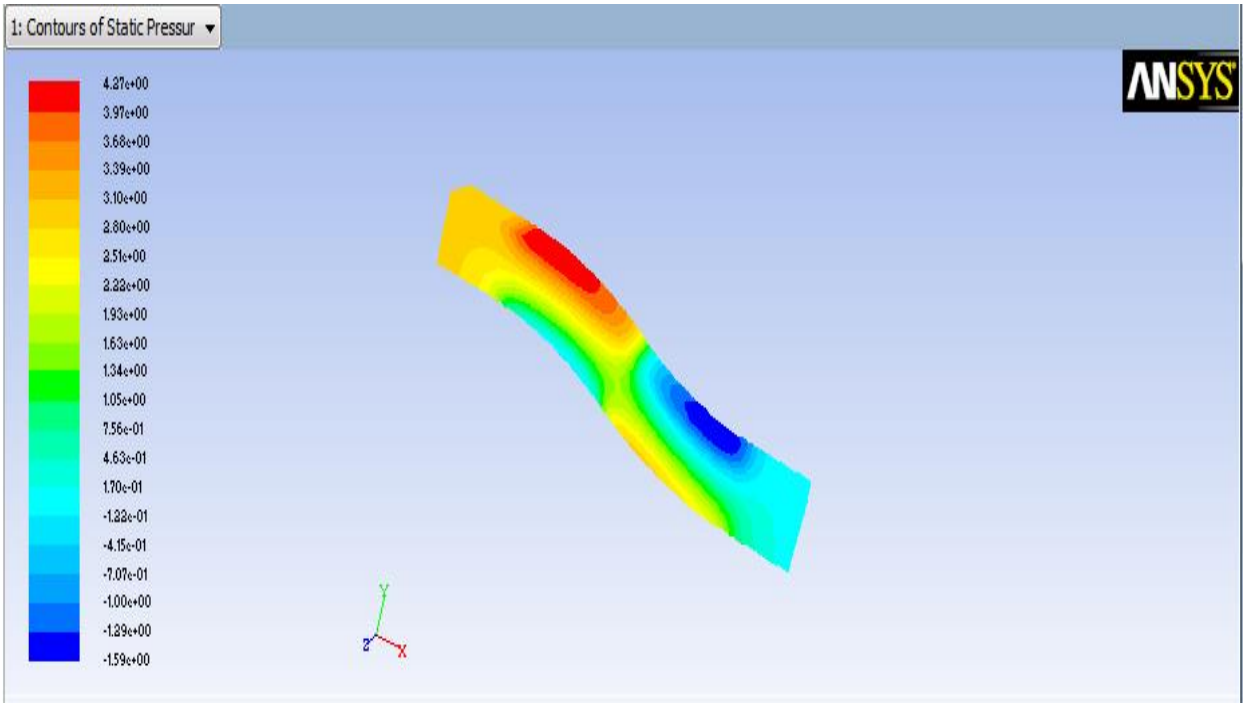

Fig: 2 Contour of Static Pressure at Re=4.73x10^4

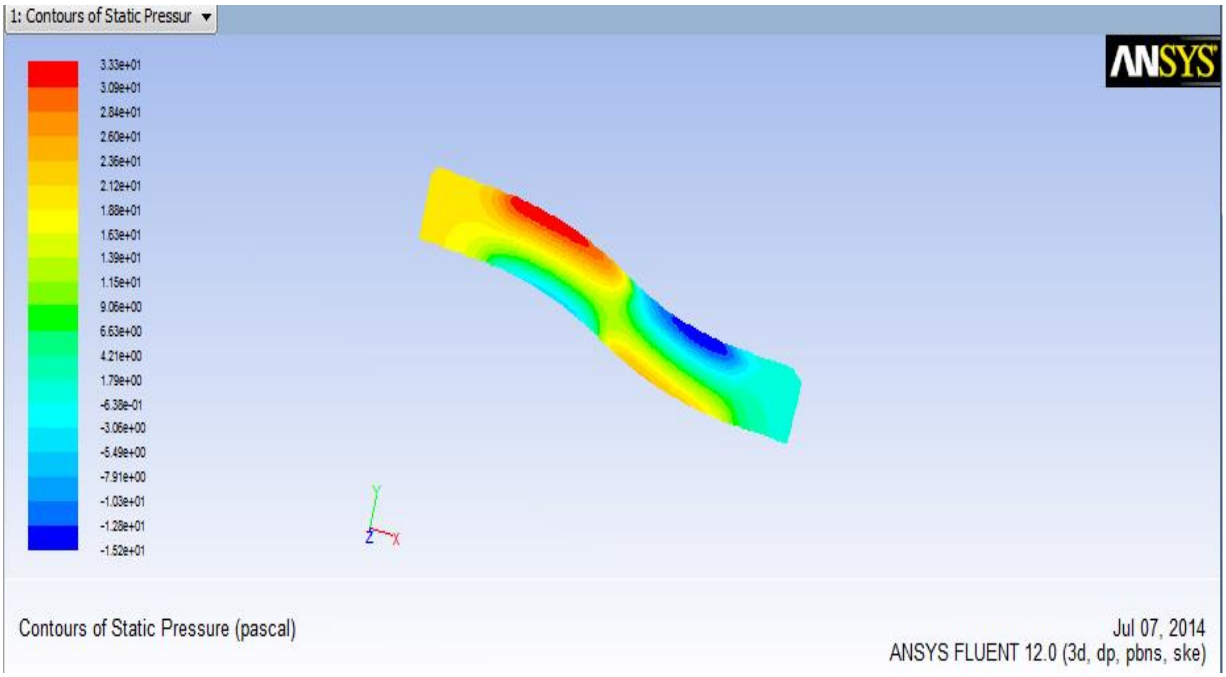

Fig: 3 Contour of static Pressure at Re=1.47x10^5

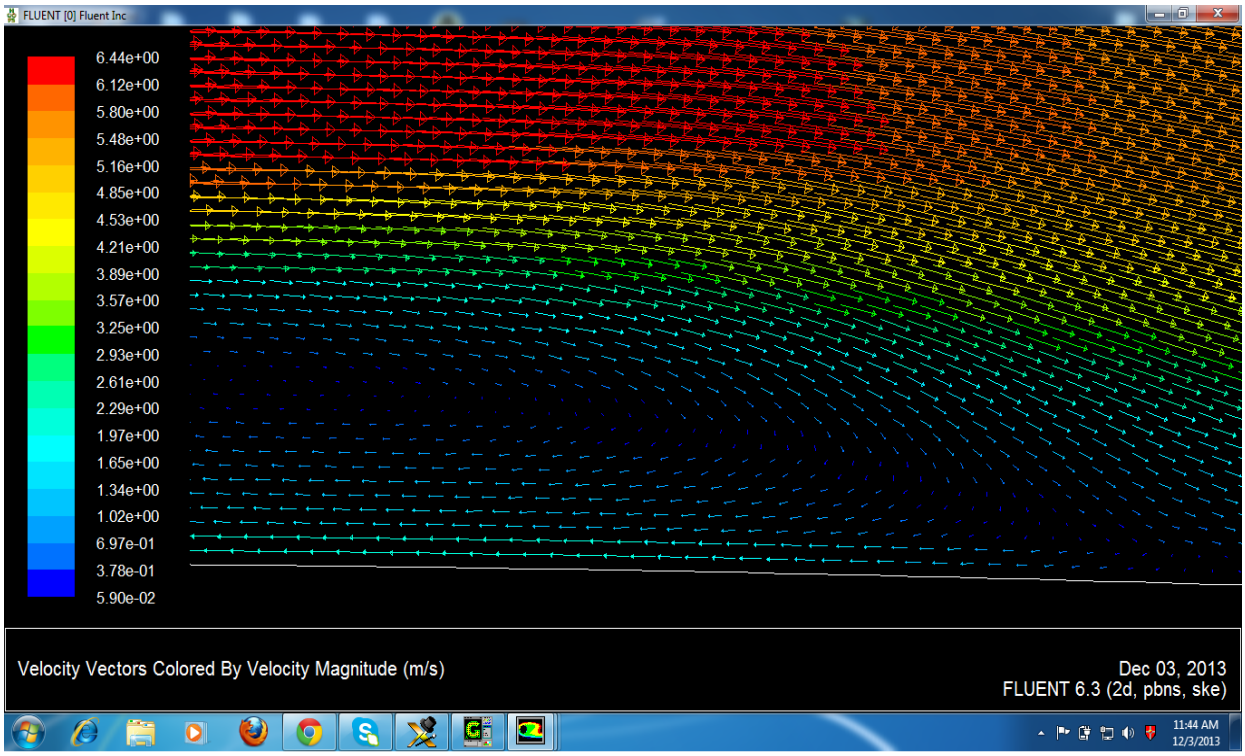

Fig: 4 Velocity vector showing flow separation.

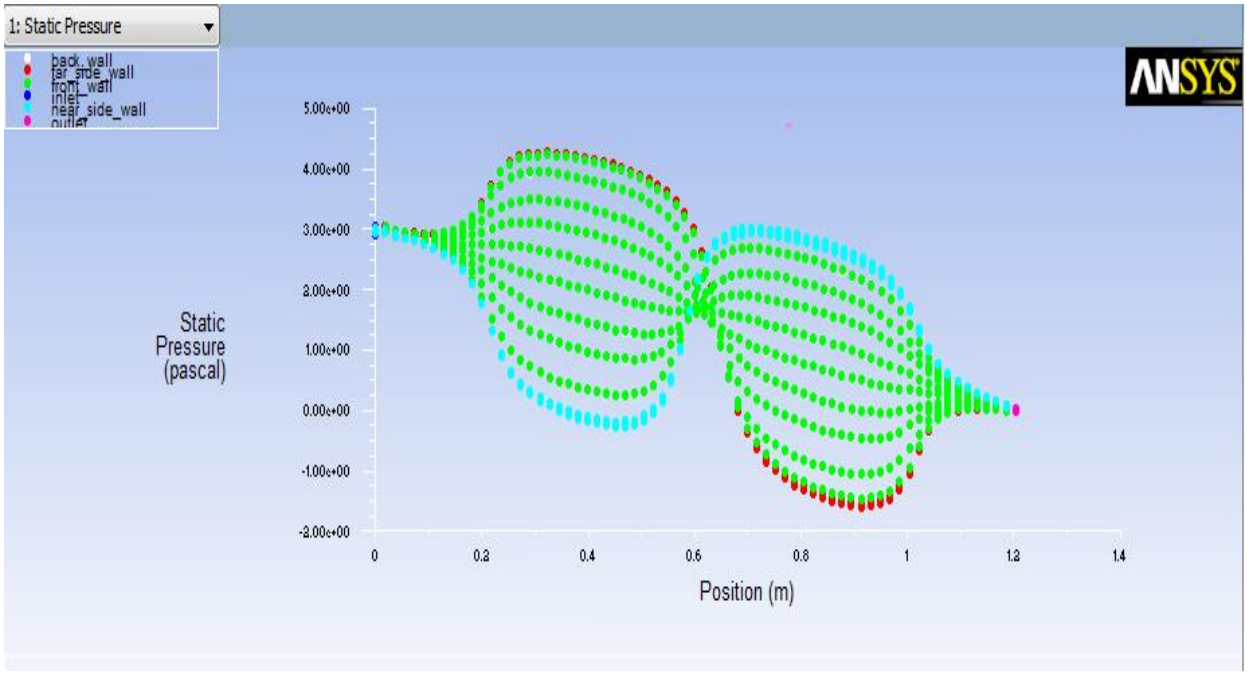

Fig: 5 Graph of static pressure v/s position

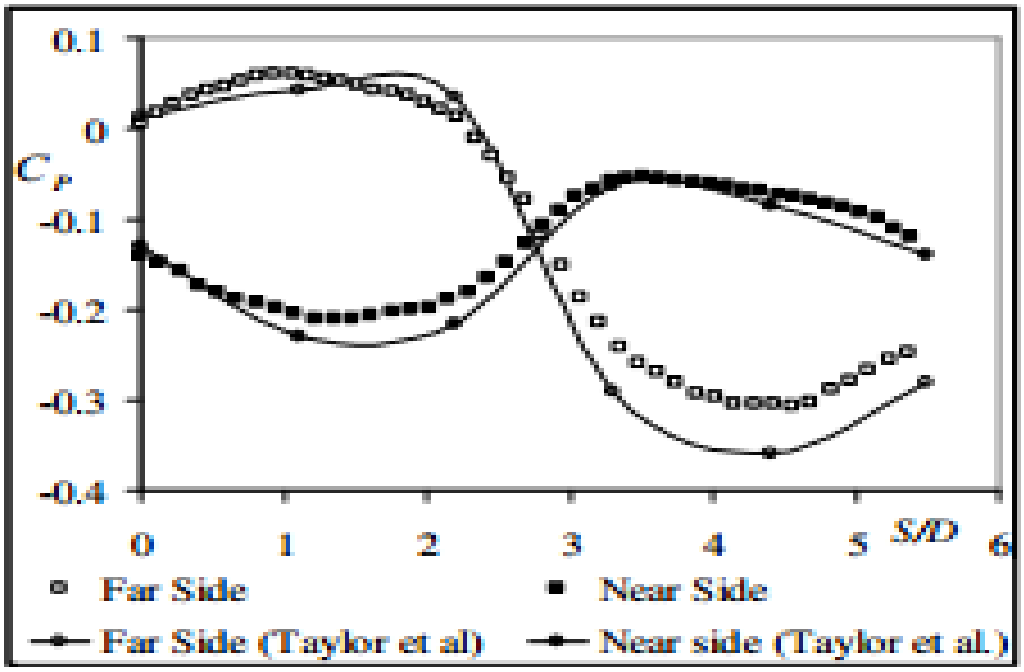

Fig: 6. Graph of Cp v/s S/D obtained practically by Taylor and Thye, N. Y.

$$C_p = \frac{p - p_0}{\rho \frac{U^2}{2}}$$

C_p= pressure coefficient

S=total stream wise distance, m.

D= hydraulic diameter, m

Table 2: Cp for side wall v/s s/d table.

S/D	C_P Far Side Wall	C_P Near Side Wall
0	0	-0.12
0.5	0.05	-0.18
1	0.08	-0.2
1.5	0.05	-0.22
2	0	-0.2
2.5	-0.05	-0.18
3	-0.15	-0.12
3.5	-0.25	-0.08
4	-0.3	-0.09
4.5	-0.35	-0.1
5	-0.3	-0.12
5.5	-0.25	-0.15

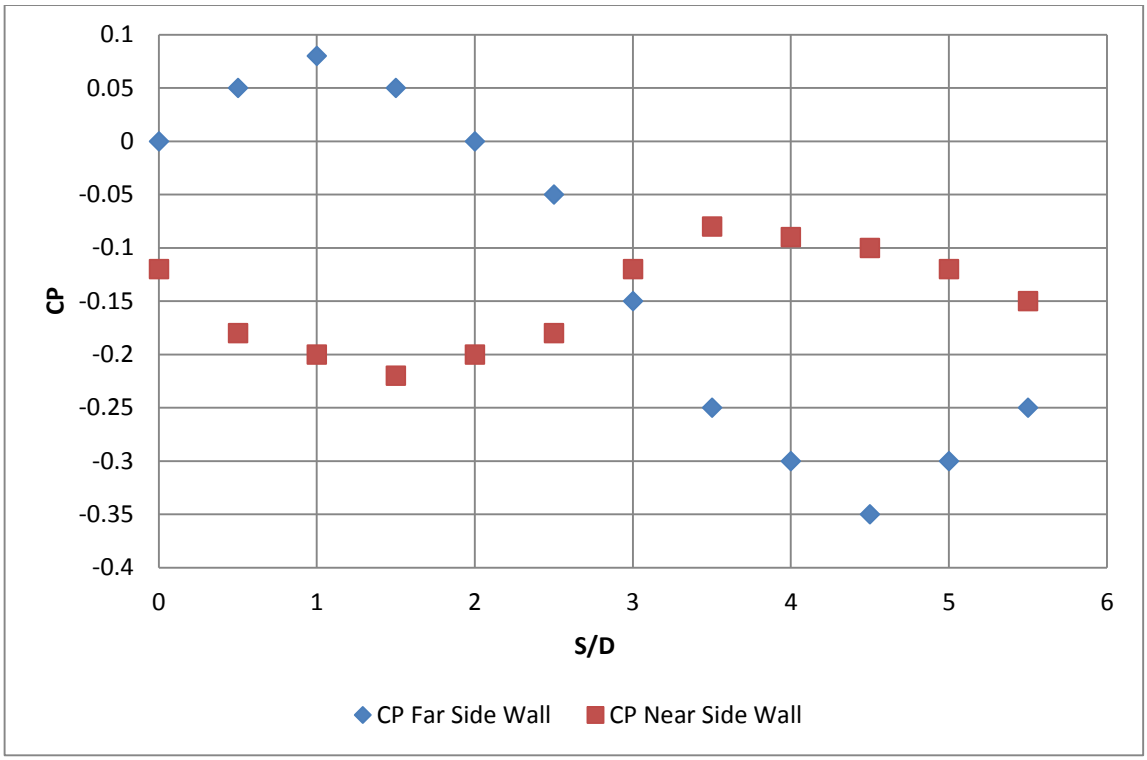

Fig: 7 Graph obtained Cp v/s S/D by simulation.

On the study of 3d s-shaped duct we found that from Fig.2 and Fig.3 i.e. contour of static pressure there are two low pressure zones are create on the duct one at near side wall of the 1st bend and other on the far side wall of the second bend. On these two pocket of the bend there is a flow separation which is clearly seen by the Fig. no.4 i.e. contour of velocity vector. For suppressing this flow separation we can use different flow control techniques. From Fig. 2 and Fig. 3 it is clearly seen that the contour of static pressure is same for both the Reynolds number only there is difference in magnitude. Fig. 5 shows that the plot of static pressure vs. position .the trend obtained from Fig.5 is clearly matched with the Fig. 6 i.e. practically result obtained by the Thye, N. Y., 2009.now from the different values obtained from the pressure graph we calculate value of Cp at different point of the duct which is shown on the Table no 2. Fig.7 shows graph obtained Cp v/s s/d by simulation which is matched by the practical result.

Study of 3D S-Shaped Duct with Flow control Techniques:

Different flow control Techniques for improving the performance of S-Duct.

- Vortex generator
- Tangential blowing

1. Study of 3D S-Shaped Duct with vortex generator:

Vortex generators " locally" mix the high momentum fluid in the free stream with the low momentum fluid near the wall and thus energies the boundary layer to suppress flow separation.

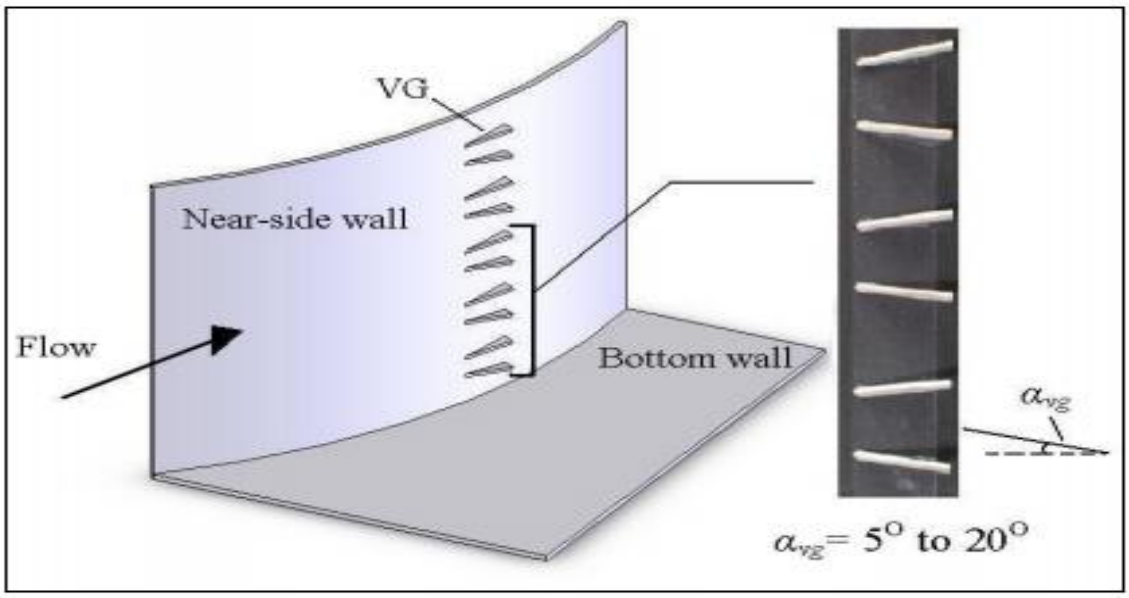

Fig: 8 vortex generator on near side wall [13]

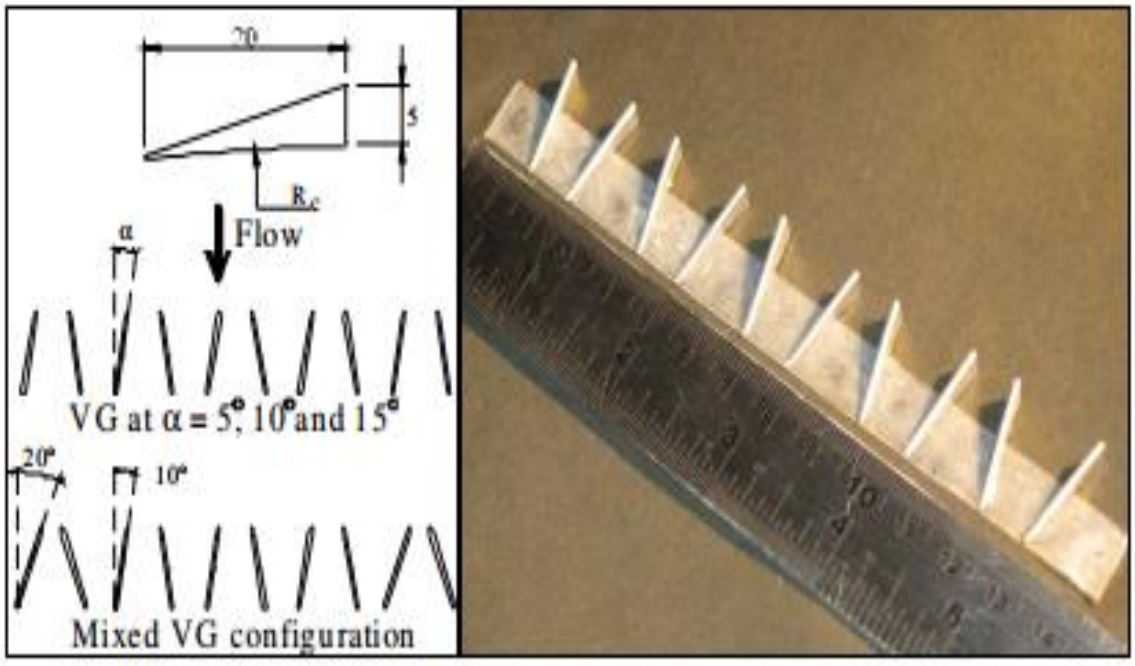

Fig: 9 Vortex generator configuration [13]

Effects of flow control devices

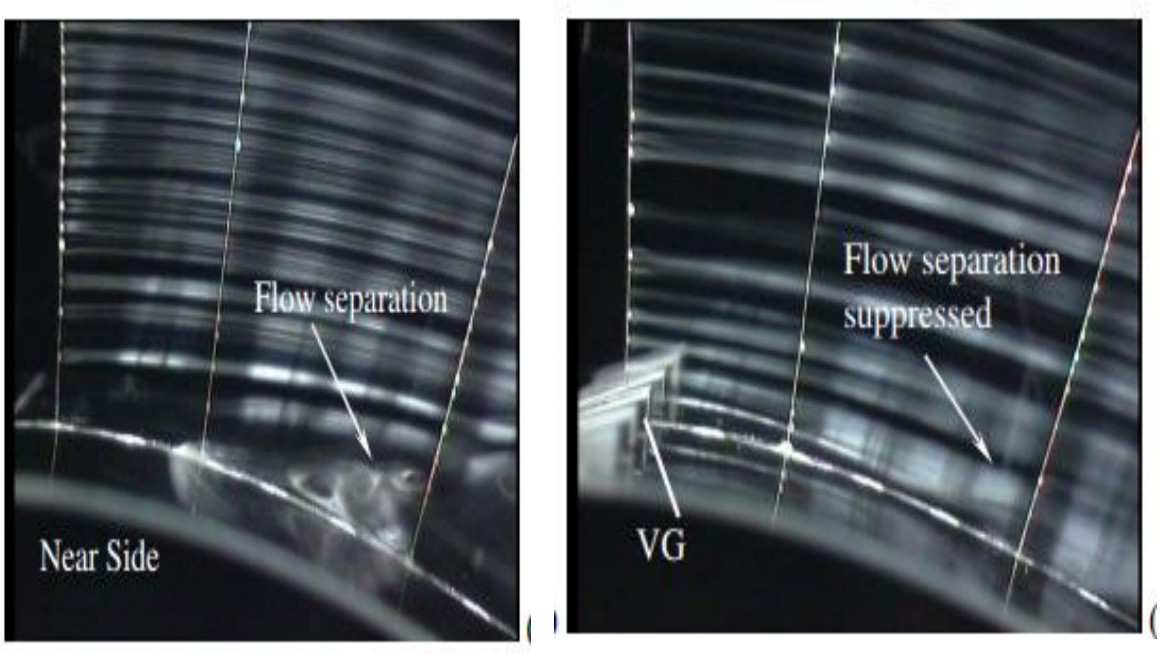

Fig: 10 shows flow separation and suppressed flow [13]

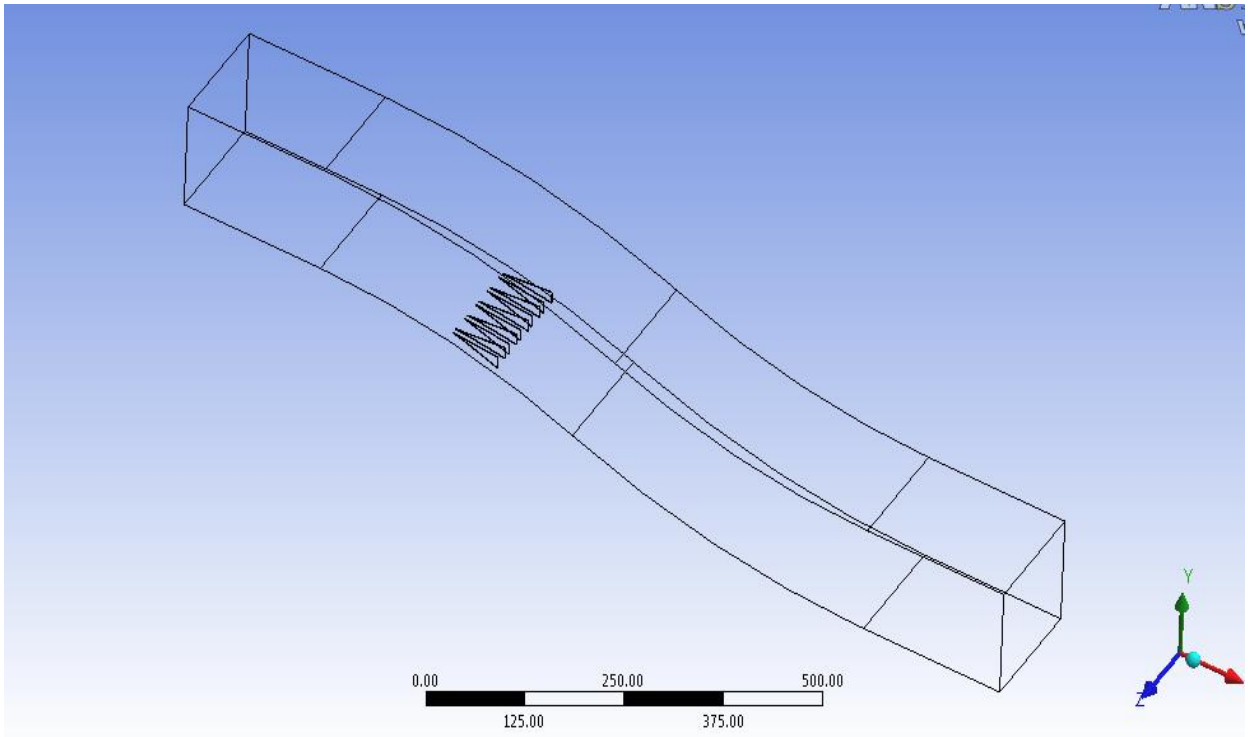

Fig: 11 s-duct with vortex generator

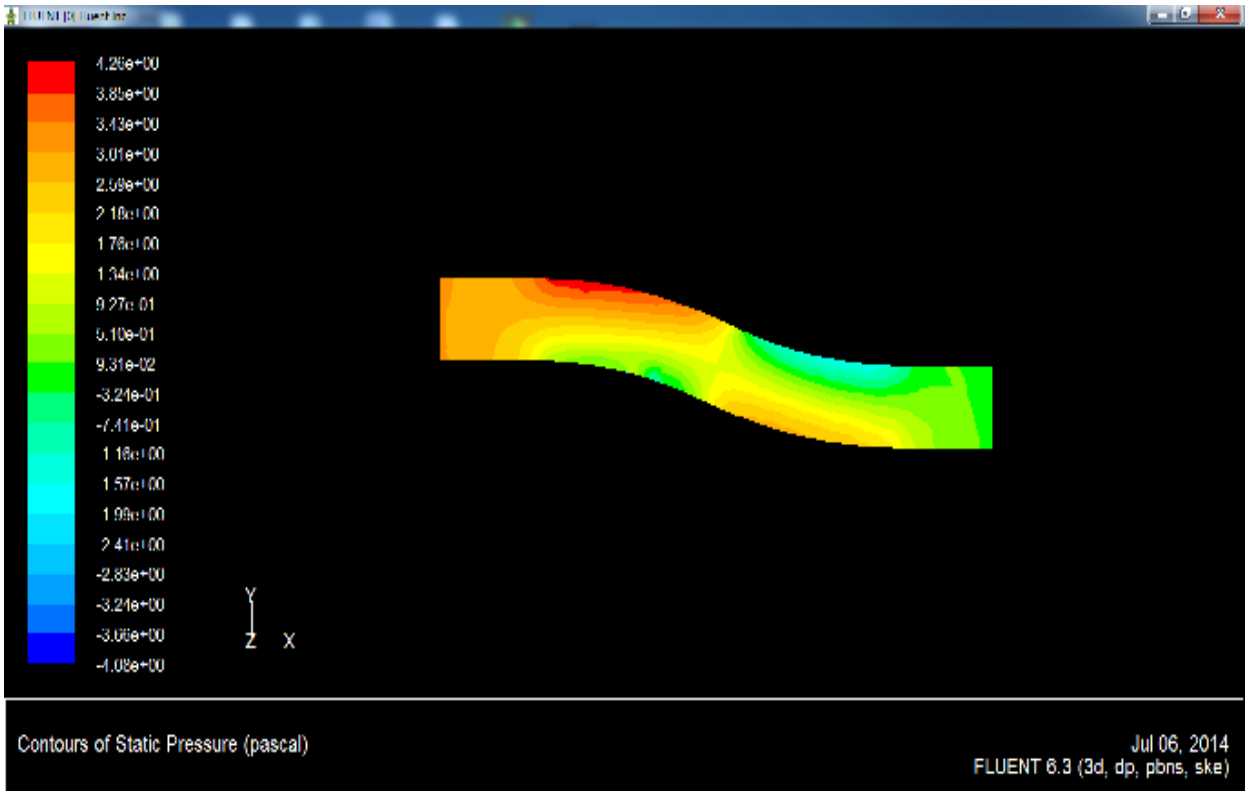

Fig: 12 contour of static pressure v/s position for *Re*=4.73x10^4

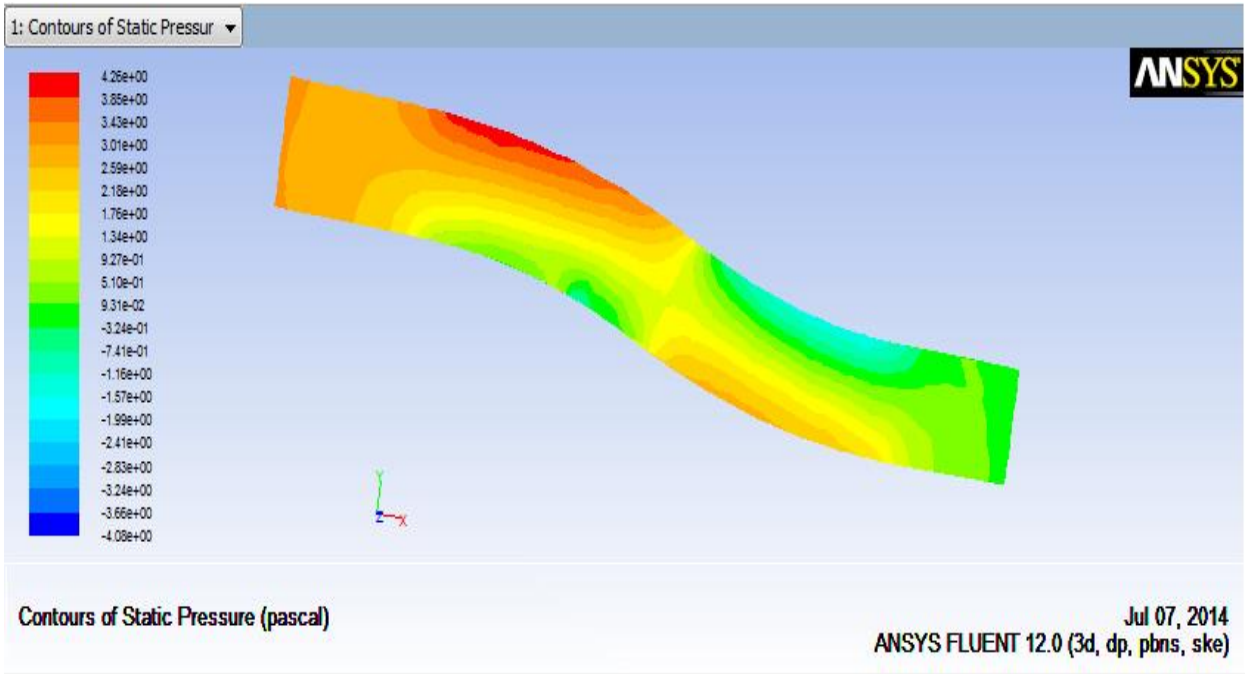

Fig: 13 contour of static pressure v/s position for *Re*=1.47x10^5

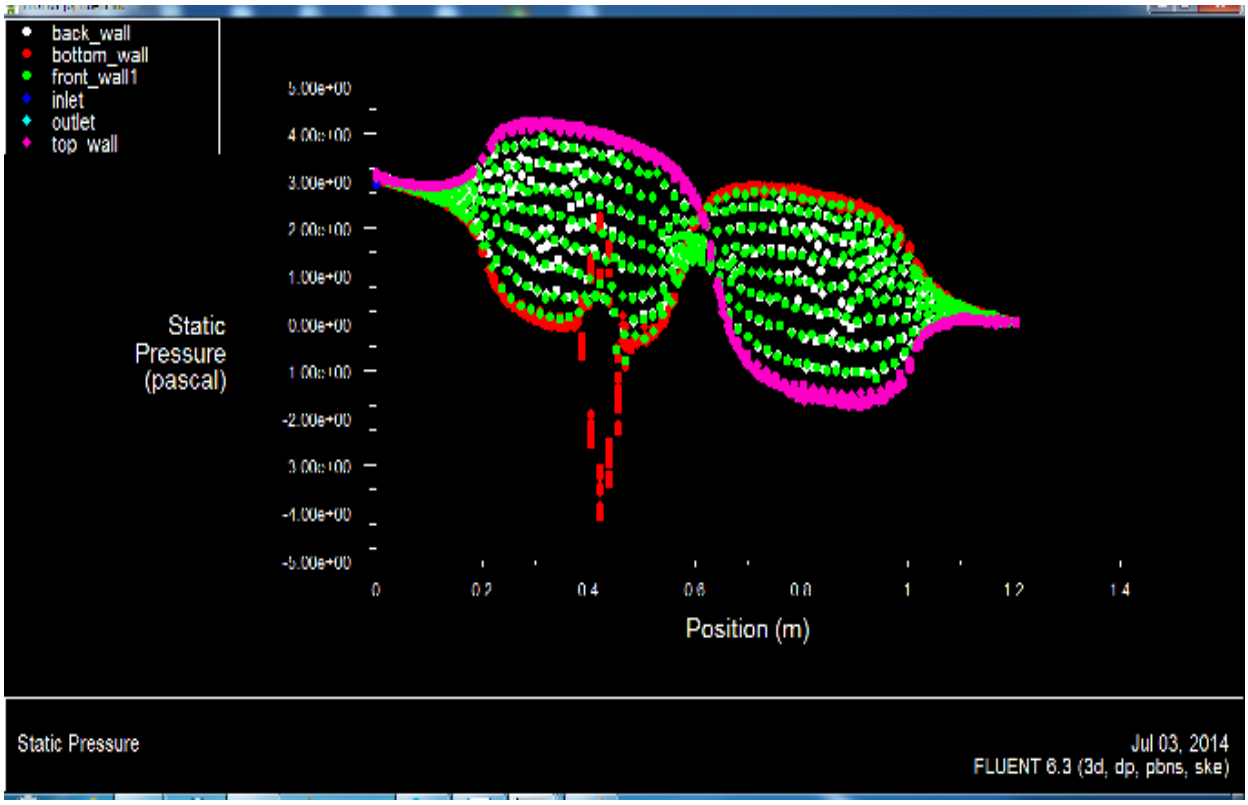

Fig: 14 Plot of static pressure v/s position

On the study of 3d S-shaped duct with flow control technique i.e. with vortex generator we found that from Fig.12 and Fig. 13 i.e. contour of static pressure there are no low pressure zones are create on the duct one at near side wall of the 1st bend and other on the far side wall of the second bend as found from the analysis from bare duct. From Fig. 12 and 13 it is clearly seen that the contour of static pressure is same for both the Reynolds number only there is difference in magnitude. Fig 14 shows that the plot of static pressure vs. position .the trend obtained from Fig. 5 is clearly matched with the Fig. 6 i.e. practically result obtained by the Thye, N. Y., 2009.now from the different values obtained from the pressure graph we calculate value of Cp at different point of the duct which is shown on the Table no 2. Fig.7 shows graph obtained Cp v/s s/d by simulation which is matched by the practical result.

2. Study of 3D S-Shaped Duct with Tangential Blowing:

Tangential blowing with configuration: Tangential Blowing uses mass addition near the separation point to energies the low momentum fluid close to the wall to overcome the adverse pressure gradient.

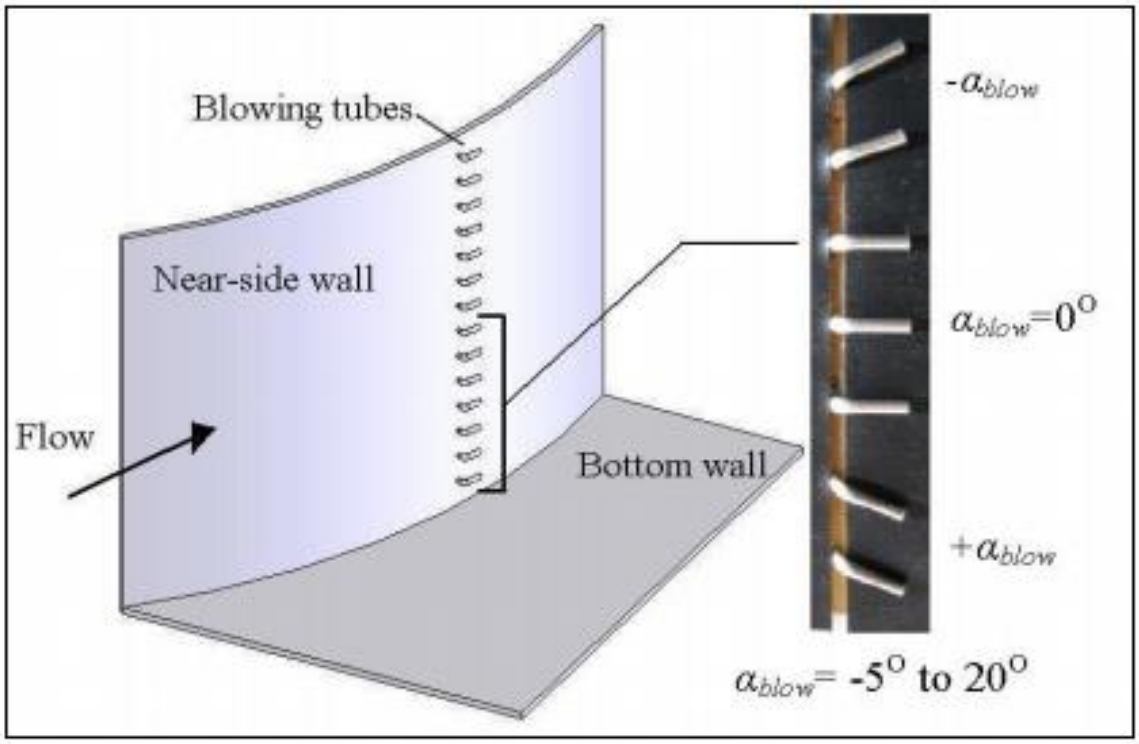

Fig: 15 configuration of blowing tubes on near side wall [13]

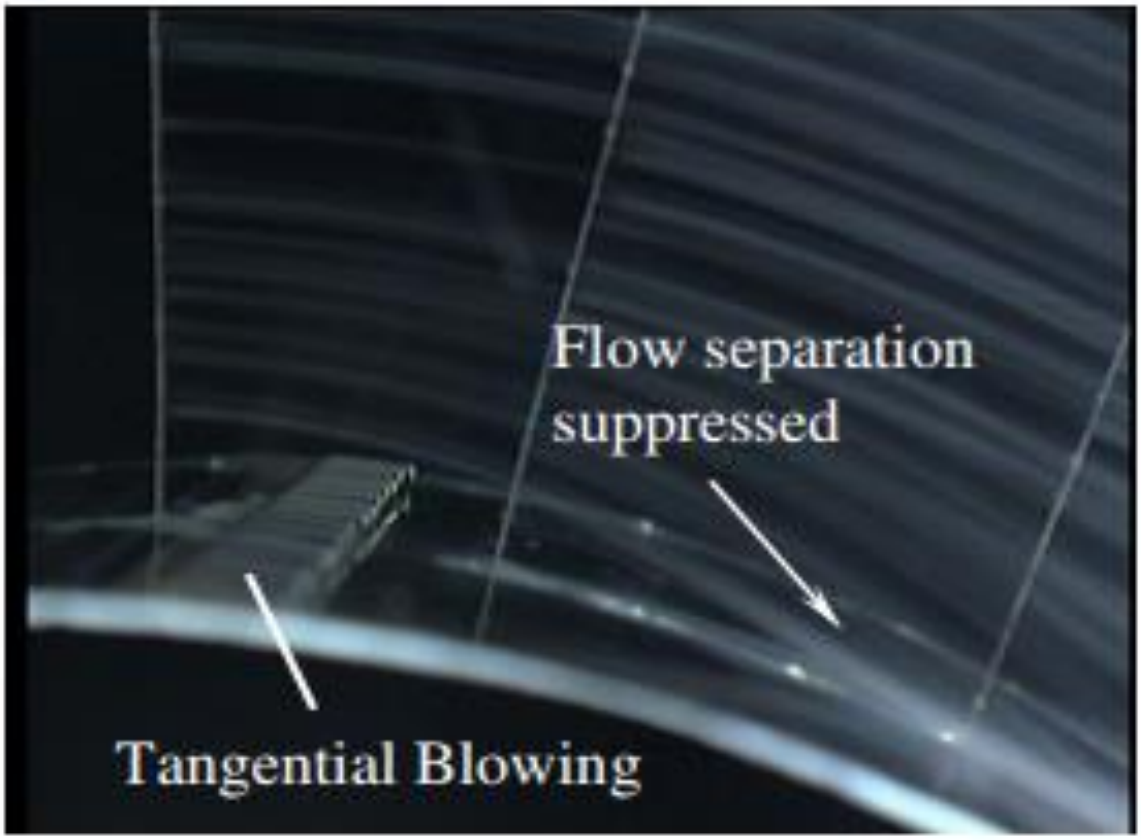

Fig: 16 shows suppressed flow experimentally [13]

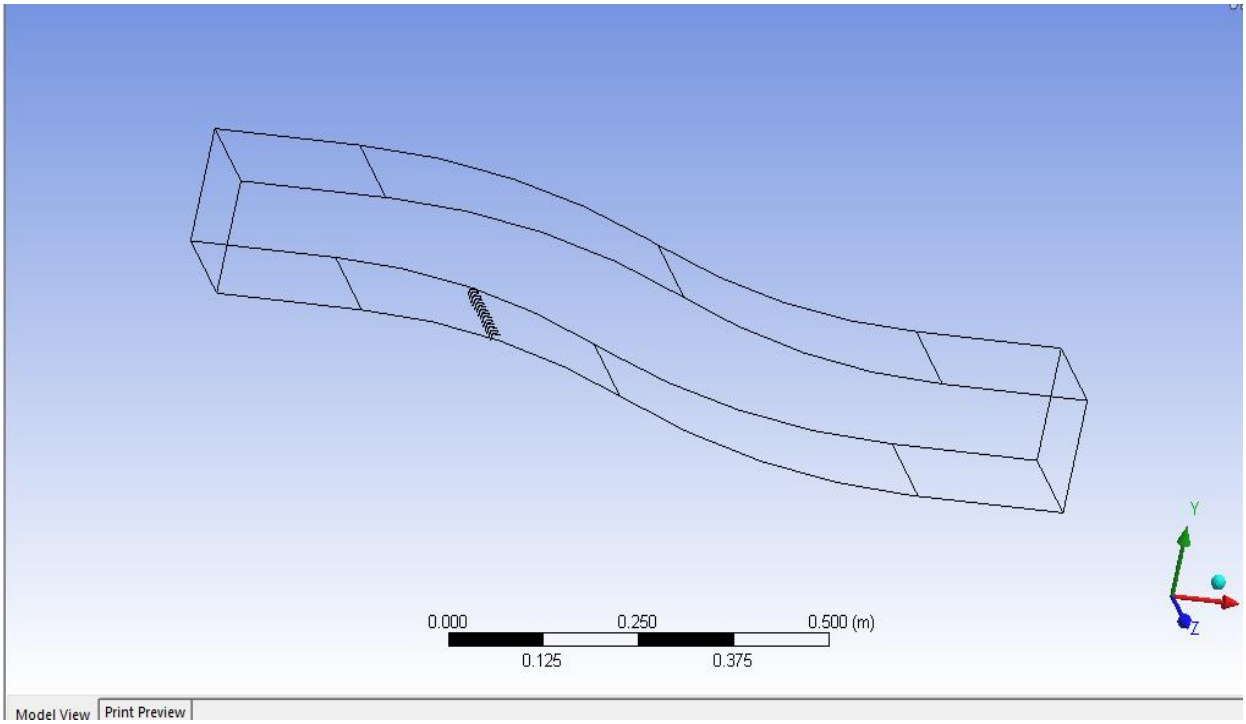

Fig: 17 S-duct with blowing tubes

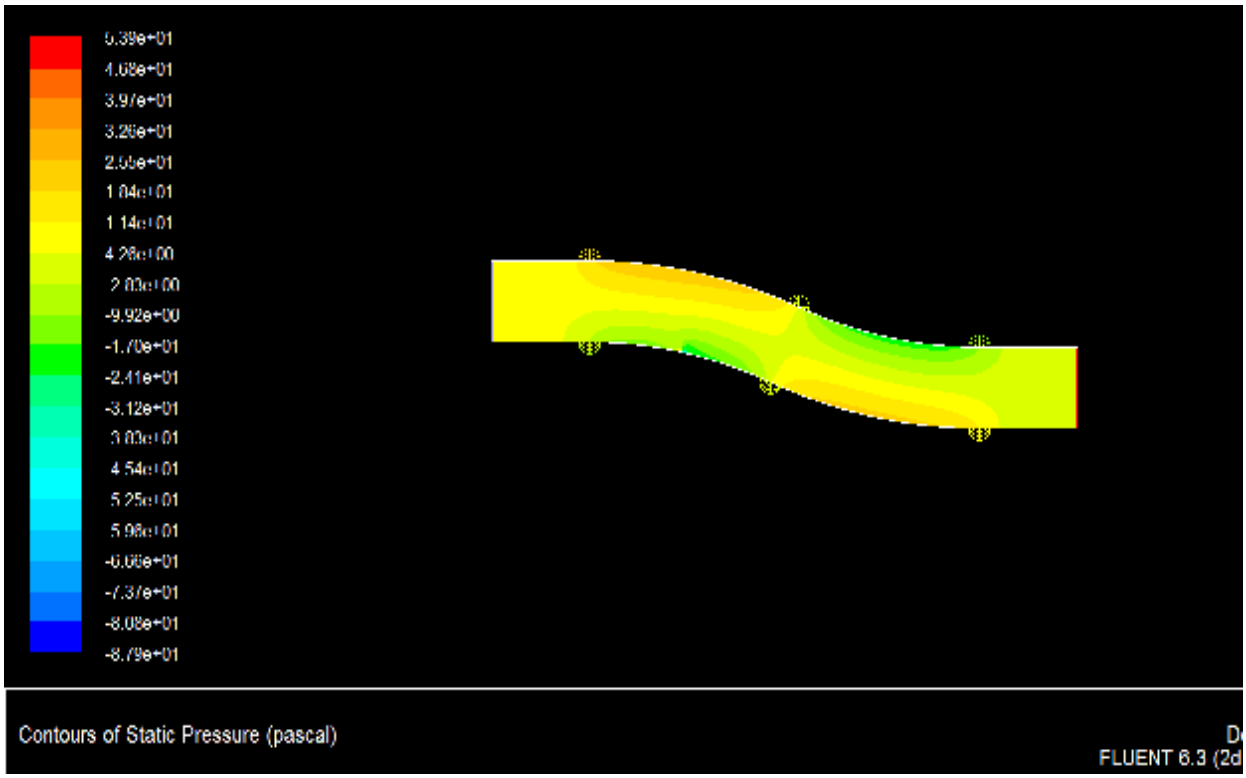

Fig: 18. Contours of static pressure with tangential blowing.

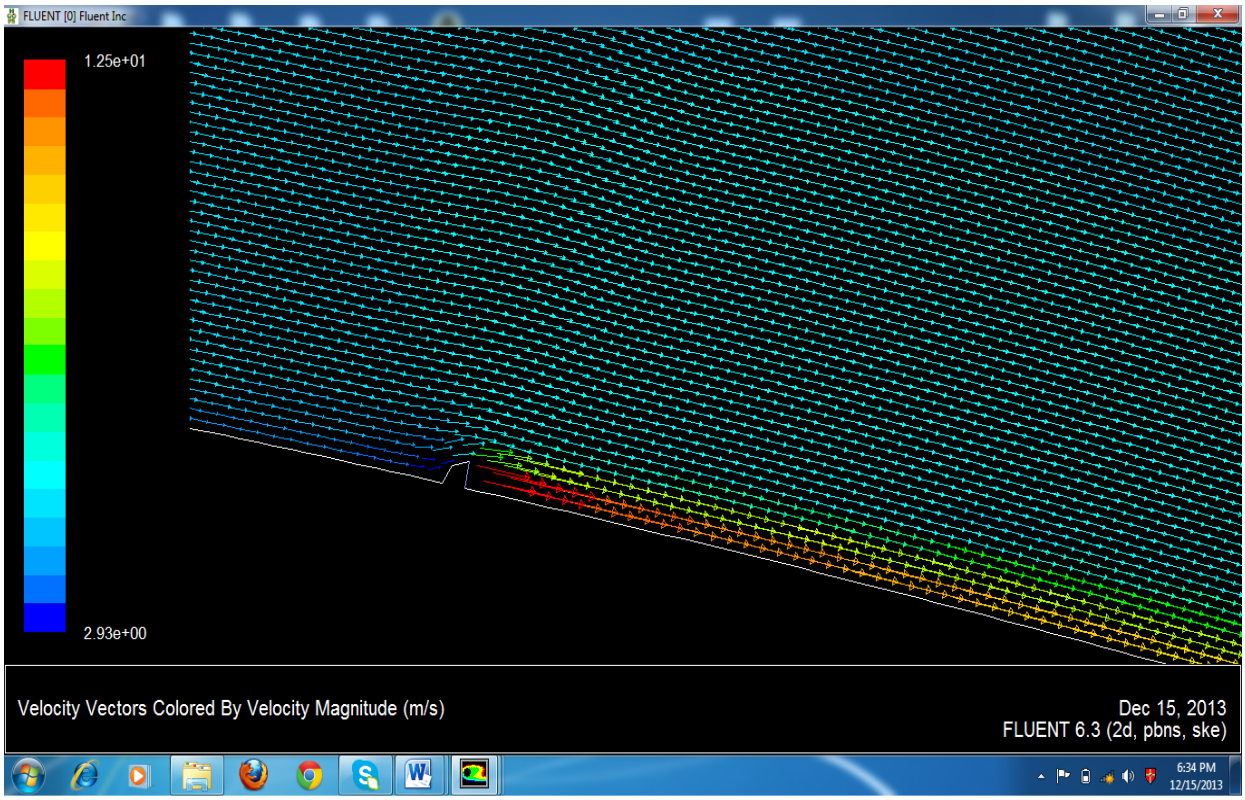

Fig: 19 Contours of velocity vector with tangential blowing.

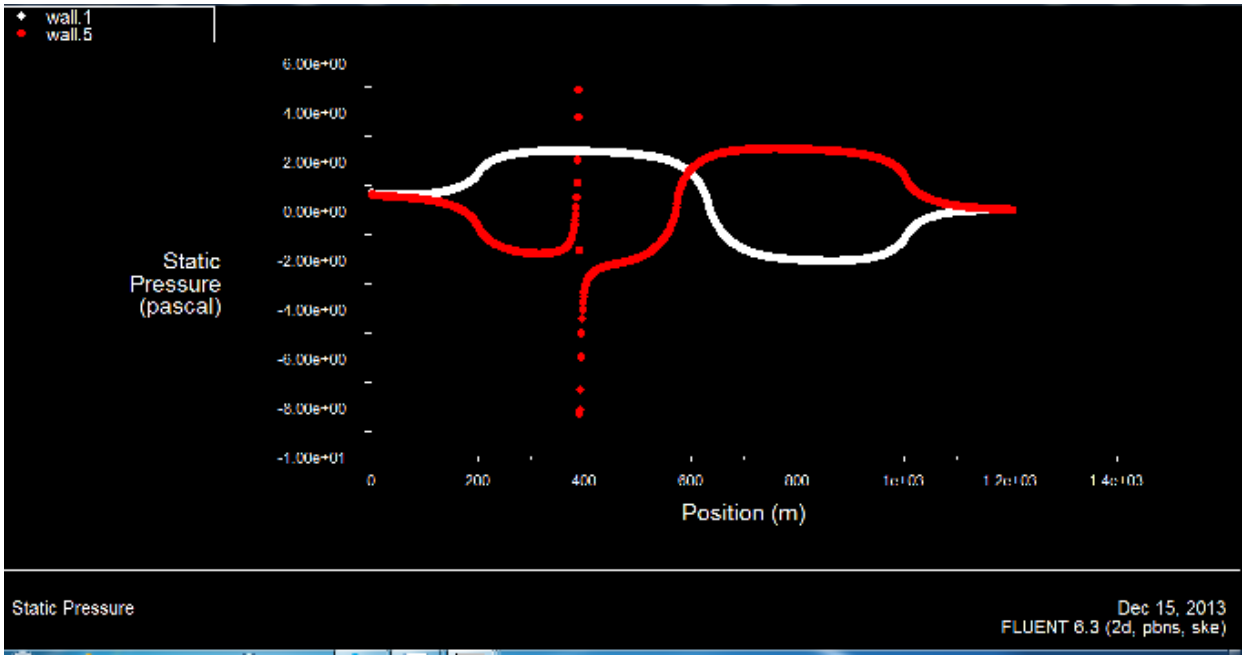

Fig: 20 Graph of static pressure v/s position with tangential blowing.

CASE-3: Contours of S-bend with Reynolds no1.47x10^{5}and tangential blowing

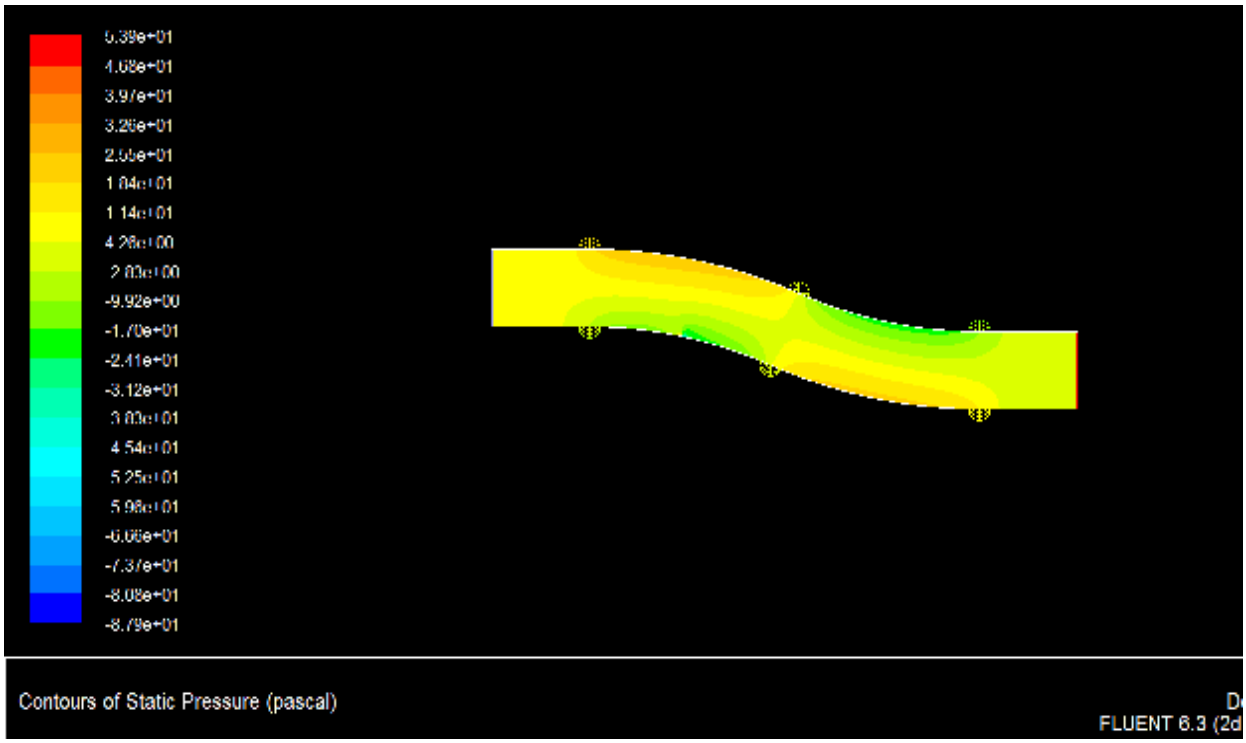

Fig: 21 Contours of static pressure with tangential blowing.

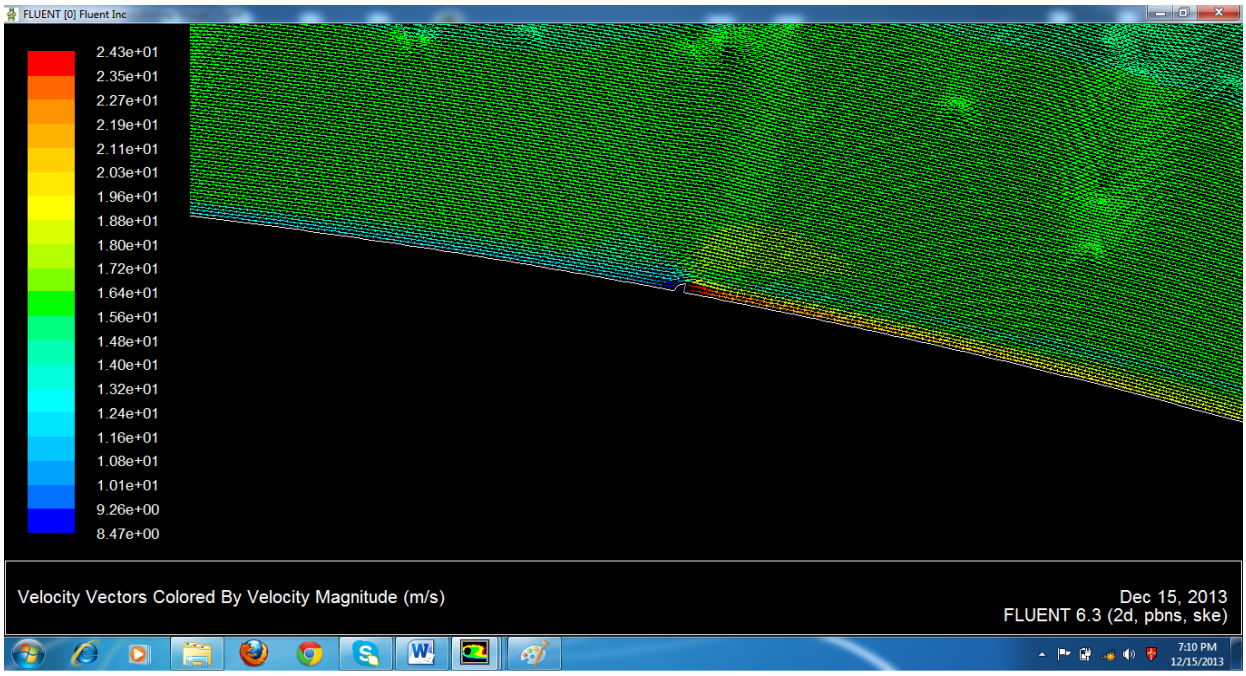

Fig: 22 Contours of velocity vector with tangential blowing.

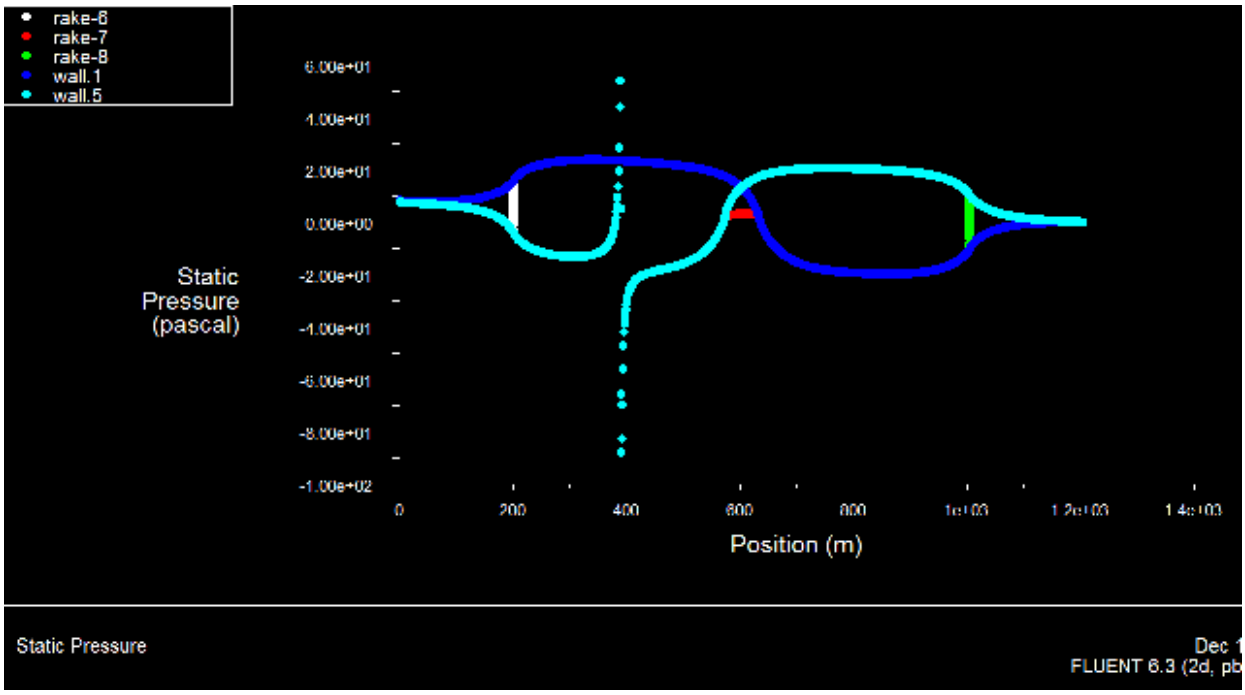

Fig: 23 static pressure v/s position graph

On the study of 3d s-shaped duct with flow control technique i.e. with tangential blowing we found that from Fig.18 and Fig.21 i.e. contour of static pressure there are no low pressure zones are create on the duct one at near side wall of the 1st bend and other on the far side wall of the second bend as found from the analysis from bare duct. From Fig.18 and 21 it is seen that the contour of static pressure is same for both the Reynolds number only there is only difference in magnitude. Fig.20 and 23 shows that the plot of static pressure vs. position .now from the different values obtained from the pressure graph we calculate value of Cp at different point of the duct which is shown on the table no 4 and 6. Fig.26 and 30 shows graph obtained Cp v/s s/d by simulation which is matched by the practical result [13].

From the above simulation results following tables and graphs are plotted for surface pressure distribution Cp and total pressure loss coefficient.

1. Table of surface pressure distribution on the side wall (far side wall and near side wall) for bare duct and duct with vortex generator at *Re*=4.73x10^4

Table.3: Surface pressure distribution on the side wall at *Re*=4.73x10^4

S/D	Cp far Side (bare)	Cp far Side (vg)	Cp Near Side (bare)	Cp Near Side (vg)
0	0.21	0.2	-0.3	-0.35
0.25	0.3	0.3	-0.45	-0.47
0.5	0.35	0.35	-0.52	-0.7
0.75	0.43	0.44	-0.55	-1

1	0.3	0.35	-0.45	-0.7
1.25	0.3	0.3	-0.5	-0.58
1.5	-0.25	-0.1	-0.5	-0.2
1.75	-0.4	-0.25	-0.2	0
2	-1.1	-0.8	-0.2	0.2
2.25	-1	-0.9	-0.01	0.25
2.5	-1.05	-0.9	0	0.25
2.75	-0.9	-0.8	0	0.25
3	-0.9	-0.7	0	0.15
3.25	-0.5	-0.6	0.2	0.2
3.5				

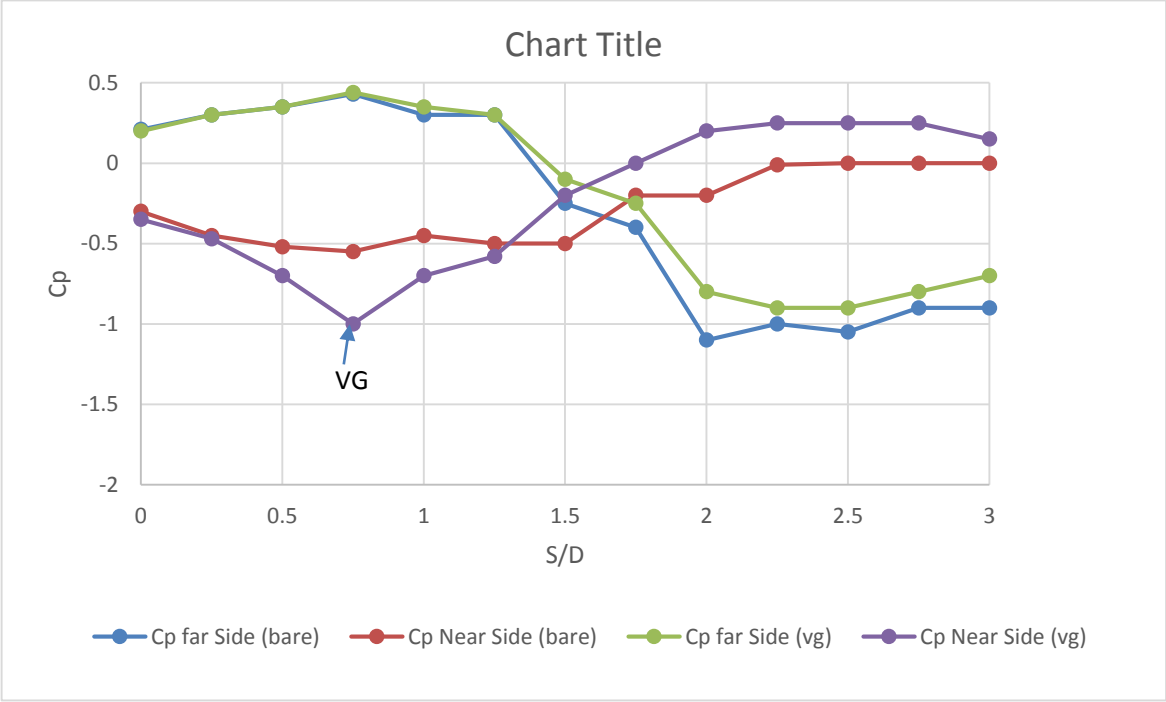

Fig: 24 Surface pressure distribution on the side wall at Re=4.73x10^4

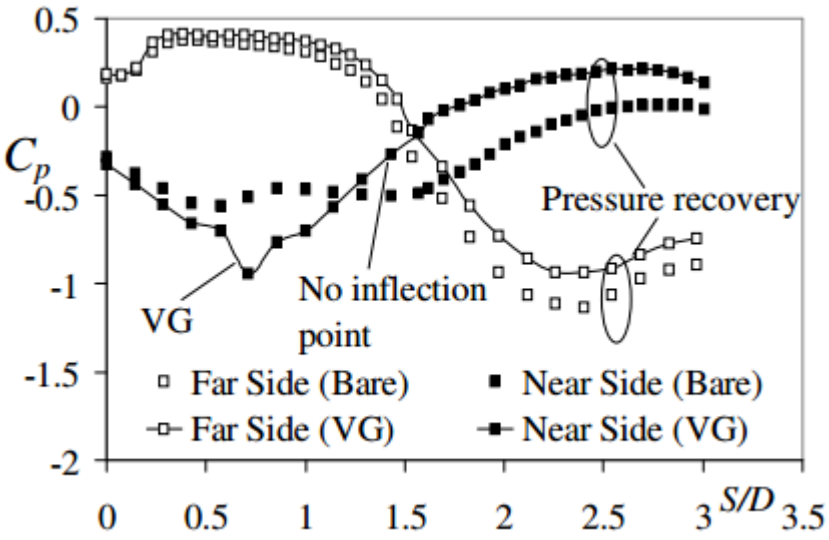

Fig: 25. Graph of Cp v/s S/D obtained practically by Thye, N. Y [13] at *Re*=4.73x10^4

From above chart it is clearly seen that there is no point of inflection in case of duct with vortex generator as compare to bare duct so it can be concluded from above chart that flow separation is suppressed by use of flow control device i.e. vortex generator.

2. Table of surface pressure distribution on the side wall (far side wall and near side wall) for bare duct and duct with Tangential blowing at *Re*=4.73x10^4

Table.4: Surface pressure distribution on the side wall at *Re*=1.47x10^5

S/D	Cp far Side (bare)	Cp far Side (blowing)	Cp Near Side (bare)	Cp Near Side (blowing)
0	0.2	0.25	-0.3	-0.35
0.25	0.3	0.3	-0.45	-0.47
0.5	0.35	0.37	-0.5	-0.71
0.75	0.43	0.44	-0.55	-0.9
1	0.3	0.35	-0.4	-0.55
1.25	0.3	0.3	-0.5	-0.3
1.5	-0.3	-0.1	-0.4	-0.1
1.75	-0.75	-0.25	0	0.3
2	-1	-0.6	-0.1	0.3
2.25	-1.2	-0.9	0.05	0.4
2.5	-1.2	-0.8	0.1	0.4
2.75	-1	-0.8	0.15	0.25
3	-0.9	-0.65	0.1	0.25
3.25	-0.5	-0.6	0.2	0.2
3.5				

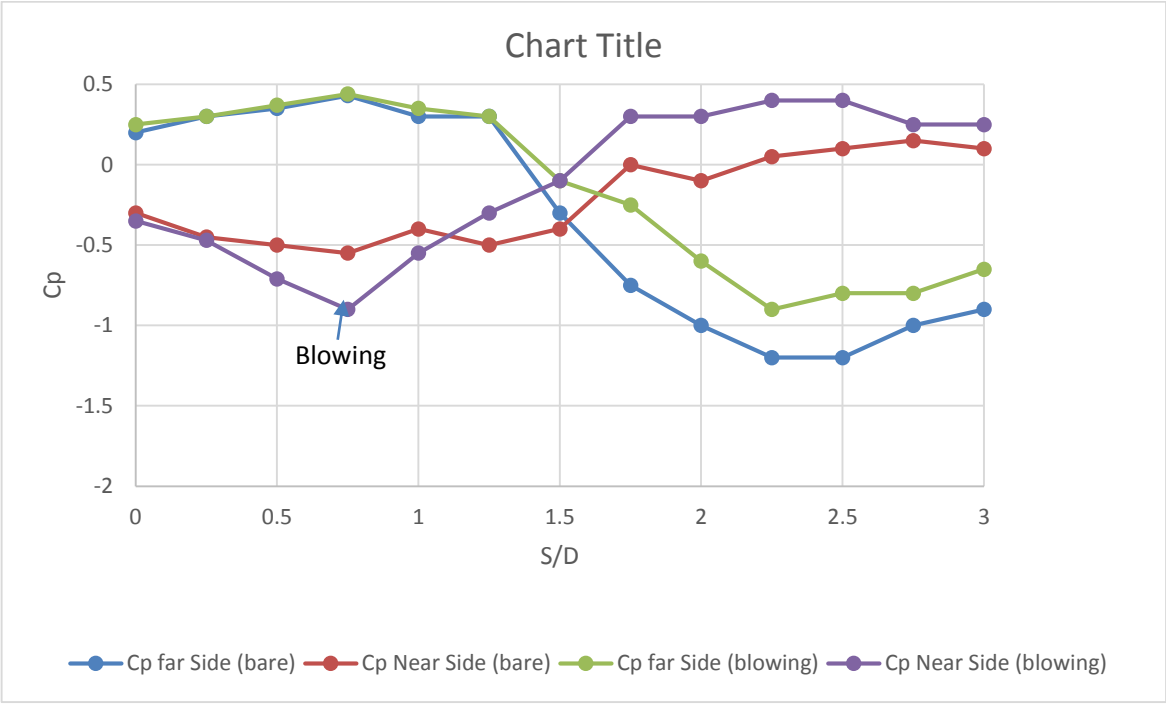

Fig: 26 Surface pressure distribution on the side wall at *Re*=4.73x10^4

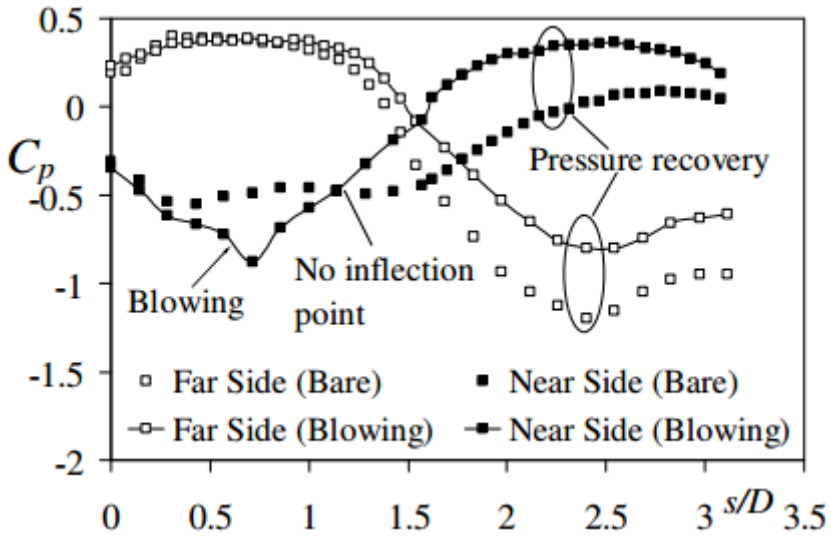

Fig: 27 Graph of Cp v/s S/D obtained practically by Thye, N. Y [13] at Re=4.73x10^4

From Fig.25 and Fig.26 it is seen that there is no point of inflection in case of duct with vortex generator as compare to bare duct so it can be concluded from above chart that flow separation is suppressed by use of flow control device i.e. vortex generator and the pattern obtained by simulation is similar to the graph of Cp vs S/D obtained practically by Thye, N. Y. i.e. Fig.27.

3. Table of surface pressure distribution on the side wall (far side wall and near side wall) for bare duct and duct with vortex generator at *Re*= 1.47×10^5

Table 5: surface pressure distribution on the side wall at *Re*=4.73×10^4

S/D	Cp far Side (bare)	Cp far Side (vg)	Cp Near Side (bare)	Cp Near Side (vg)
0	0.3	0.3	-0.35	-0.35
0.25	0.3	0.3	-0.45	-0.47
0.5	0.45	0.45	-0.65	-0.65
0.75	0.43	0.44	-0.55	-0.9
1	0.4	0.4	-0.6	-0.65
1.25	0.3	0.3	-0.5	-0.55
1.5	-0.1	-0.05	-0.05	0
1.75	-0.3	-0.25	0.28	0.3
2	-0.65	-0.6	0.25	0.25
2.25	-0.92	-0.9	0.35	0.4
2.5	-0.9	-0.9	0.35	0.3
2.75	-0.82	-0.8	0.25	0.25
3	-0.7	-0.7	0.25	0.2
3.25	-0.5	-0.6	0.2	0.2
3.5				

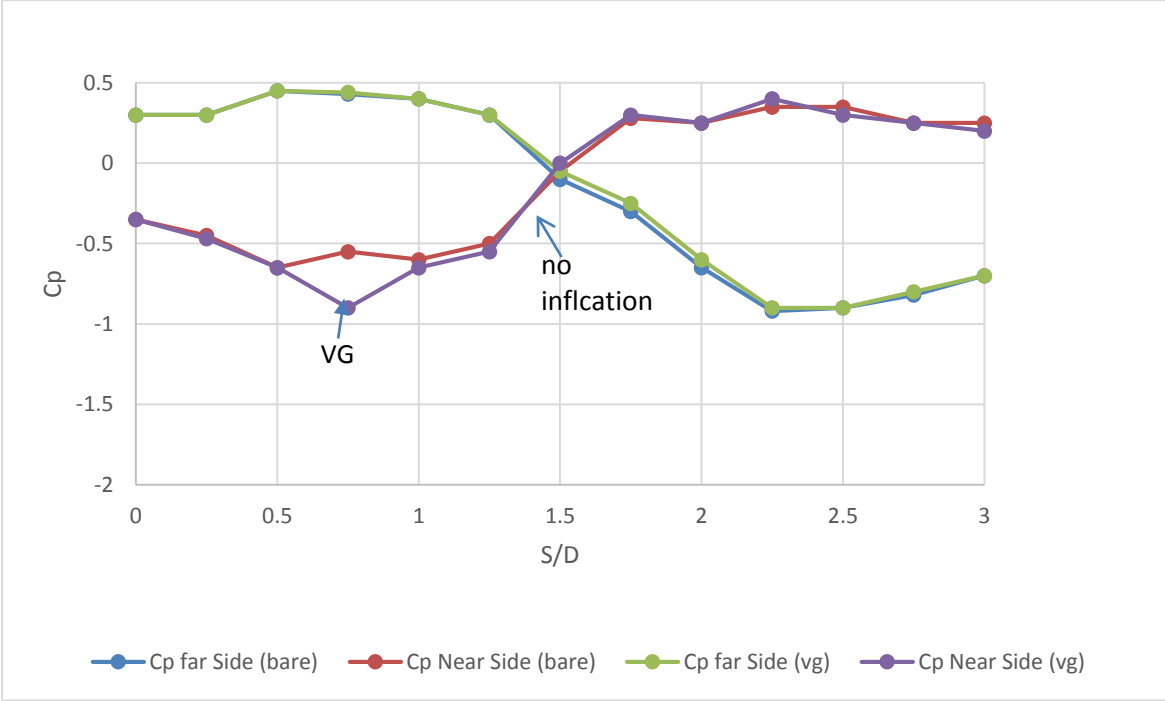

Fig: 28 surface pressure distribution on the side wall at *Re*=1.47×10^5

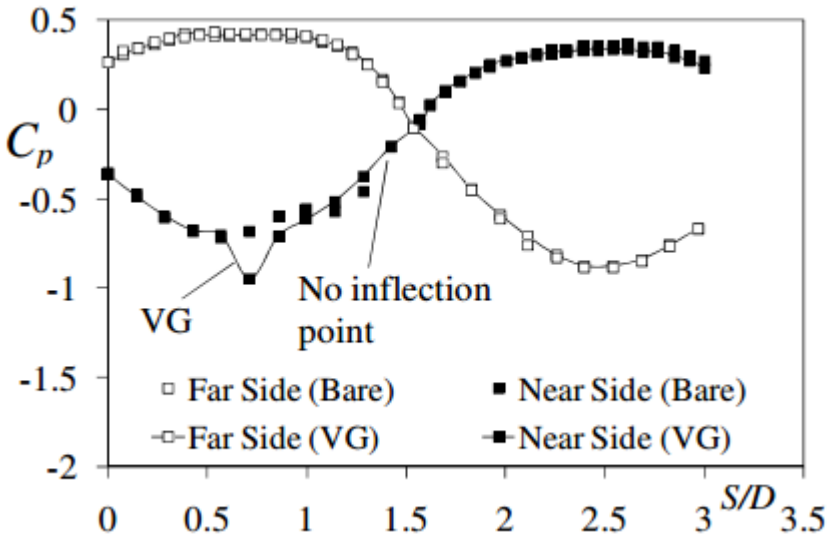

Fig: 29. Graph of Cp v/s S/D obtained practically by Thye, N. Y [13] *Re*=1.47x10^5

4. Table of surface pressure distribution on the side wall (far side wall and near side wall) for bare duct and duct with Tangential blowing at *Re*= 1.47x10^5

Table.6: surface pressure distribution on the side wall at *Re*=1.47x10^5

S/D	Cp far Side (bare)	Cp far Side (blowing)	Cp Near Side (bare)	Cp Near Side (blowing)
0	0.25	0.25	-0.25	-0.35
0.25	0.3	0.3	-0.45	-0.47
0.5	0.45	0.37	-0.67	-0.71
0.75	0.43	0.44	-0.55	-0.9
1	0.4	0.42	-0.5	-0.6
1.25	0.3	0.3	-0.35	-0.3
1.5	0	0	-0.15	-0.15
1.75	-0.3	-0.25	0	0.05
2	-0.75	-0.6	0.2	0.17
2.25	-1	-0.9	0.35	0.4
2.5	-0.85	-0.8	0.3	0.27
2.75	-0.85	-0.8	0.25	0.25
3	-0.7	-0.65	0.25	0.2
3.25	-0.5	-0.6	0.2	0.2
3.5				

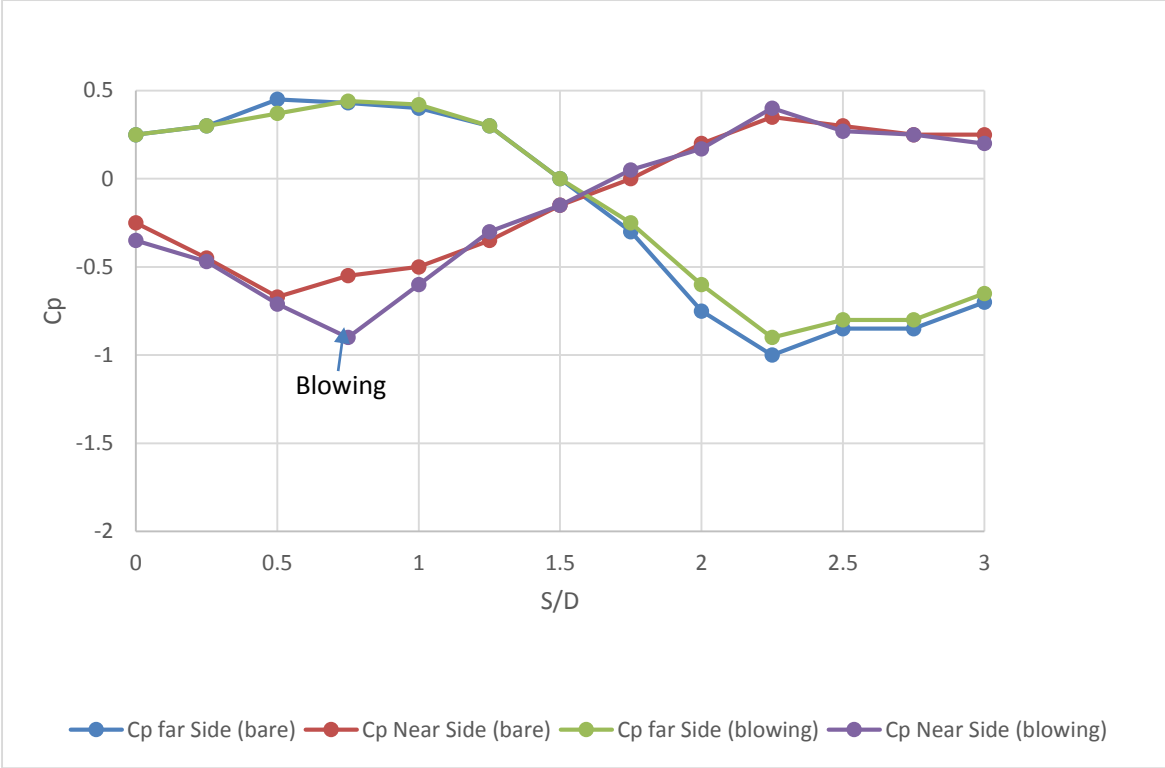

Fig: 30 surface pressure distribution on the side wall at *Re*=1.47x10^5

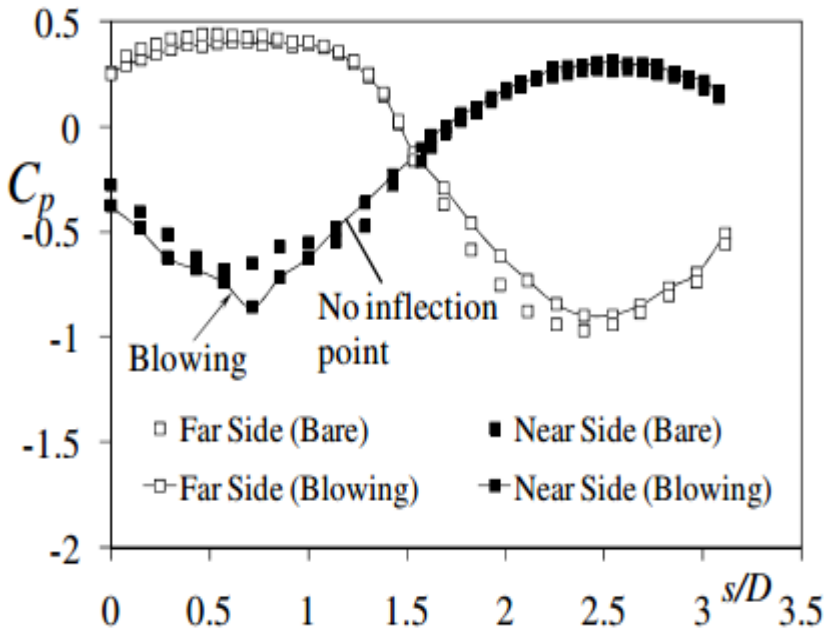

Fig: 31. Graph of Cp v/s S/D obtained practically by Thye, N. Y [13] at *Re*=1.47x10^5

From Fig.28 and Fig.30 it is seen that there is no point of inflection in case of duct with vortex generator as compare to bare duct at Re=1.47 X 10^5 so it can be concluded from above chart that flow separation is suppressed by use of flow control device i.e. Tangential Blowing and the

pattern obtained by simulation is similar to the graph of Cp vs S/D obtained practically by Thye, N. Y. i.e. Fig. 31

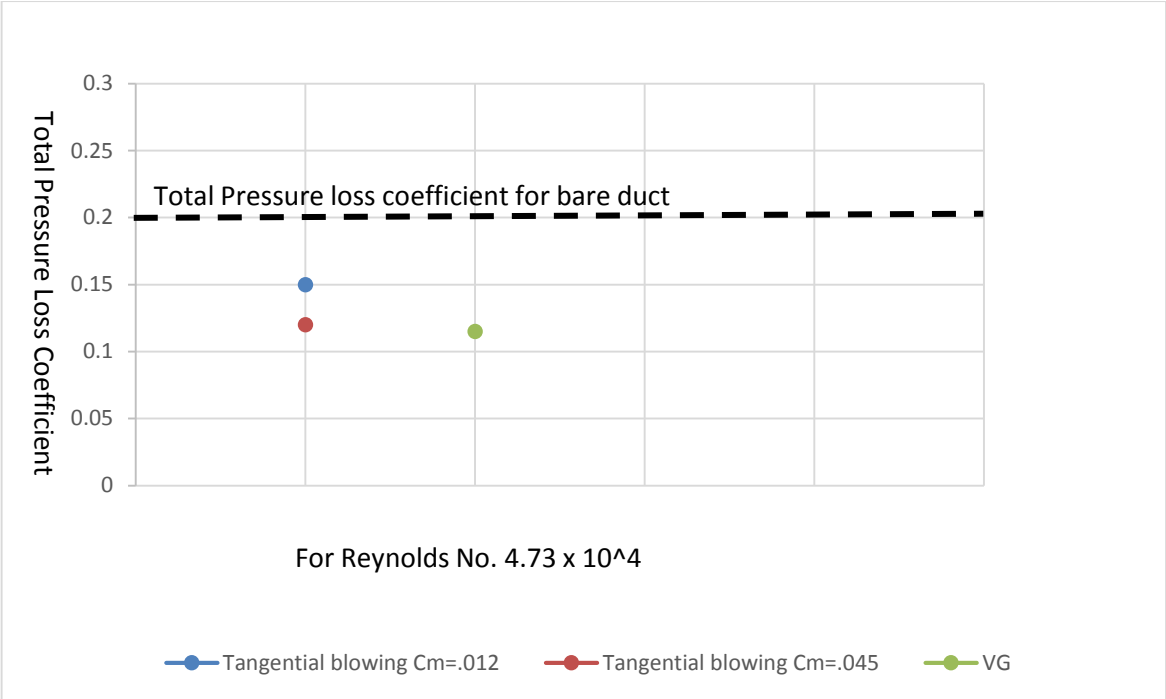

Fig: 32 Variation of total pressure loss coefficient at different incident angle for VG and Tangential blowing configuration at Re = $4.73x10^4$

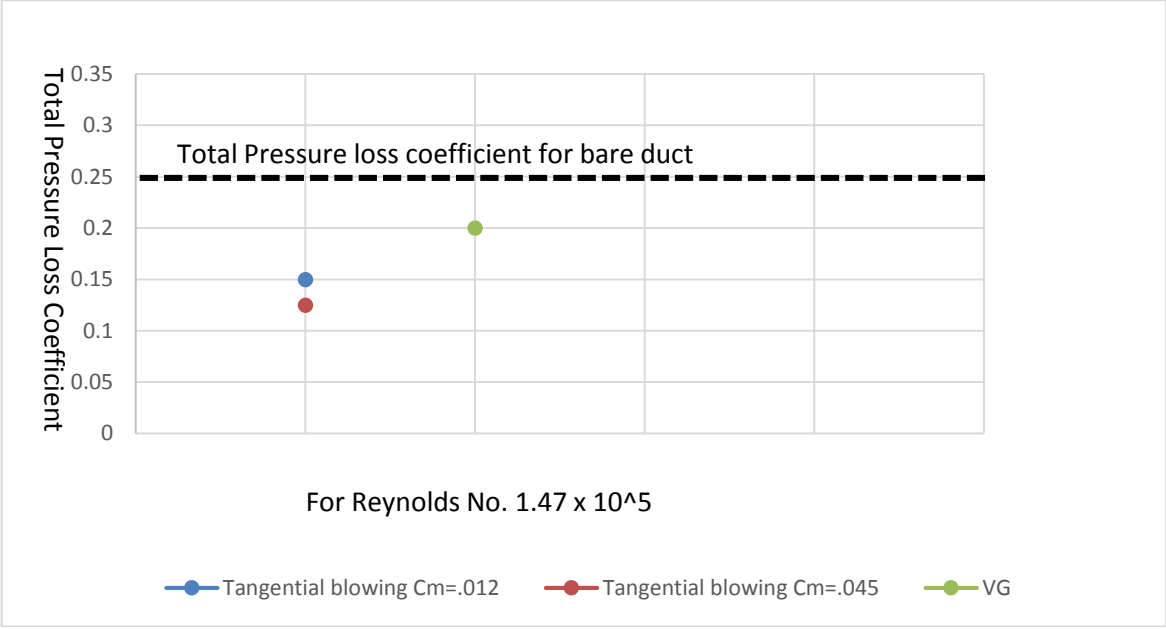

Fig: 33 Variation of total pressure loss coefficient at different incident angle for VG and Tangential blowing configuration at Re = $1.47x10^5$

Total pressure loss:

From Fig. 32 i.e. Variation of total pressure loss coefficient at different incident angle for VG and tangential blowing configuration at Re = $4.73x10^4$ and from Fig. 33 Variation of total pressure loss coefficient at different incident angle for VG and tangential blowing configuration at Re = $1.47x10^5$ it is found that there is reduction in total pressure loss coefficient by using vortex generator and tangential blowing. As total loss coefficient is 0.25 and 0.2 for the bare duct for respective Reynolds number.

In case of vortex generator it is 0.115 and in case of tangential blowing total pressure loss coefficient is 0.15 and 0.12. For Re=$4.73x10^4$.

For Reynolds number $1.473x10^5$ for vortex generator it is 0.2 and for tangential blowing 0.15 and 0.125 for respective Cm.

5. CONCLUSION

The optimum aerodynamic performance of S-shaped ducts (or aircraft air-intake ducts) demands that a relatively uniform flow with a smallest possible pressure loss. The contour of static pressure obtained from simulation of bare Duct, shows two low pressure zones are developed on the duct, one at near side wall of the 1st bend and other on the far side wall of the second bend. There is a flow separation in these two pockets of the bend which is clearly seen on the contour of velocity vector (Fig. 6).As we use two Reynolds number the effect is same, only difference in magnitude observed. Two flow control techniques namely Vortex generator and Tangential blowing are used to suppress the flow separation there why reducing total pressure loss.

The effectiveness of VGs and tangential blowing to control flow separation, reduce total pressure loss is studied. Vortex generators " locally" mix the high momentum fluid in the free stream with the low momentum fluid near the wall and thus energies the boundary layer to suppress flow separation. The graph of Cp vs S/D (Fig.24) of simulation shows no point of inflection i.e. there is no flow separation on these walls. There is also reduction in total pressure loss coefficient by using vortex generator shown in Fig. 32. As total loss coefficient is 0.25 and 0.2 for the bare duct for respective Reynolds number. In the case of vortex generator it is 0.115 and 0.2 for respective Reynolds number.

Tangential Blowing uses mass addition near the separation point to energies the low momentum fluid close to the wall to overcome the adverse pressure gradient. The Graph of Cp vs S/D(Fig 26) of tangential blowing obtained by simulation shows no point of inflection i.e. it also suppressed the flow separation. There is also reduction in total pressure loss coefficient by using Tangential blowing shown in Fig. 33. As total loss coefficient is 0.25 and 0.2 for the bare duct for respective Reynolds number. In the case of blowing when Cm is 0.012 it is 0.15 and when Cm is 0.045 it is 0.12 for Reynolds number 4.73×10^4 while it is 0.15 and 0.125 for respective Cm for Reynolds number $1.47 \times 10^{5.}$

The two methods vortex generator and Tangential Blowing were shown to be effective in suppressing flow separation and reducing total pressure loss . Therefore the results indicates competing parameters for improving the performance of flow in S-ducts.

5.1 SCOPE OF FUTHURE WORK:

Study is needed for various s-bend configurations with larger angle and swirl phenomenon in the duct. Also the condition of exit flow can be analyzed for different duct configuration. In the FLUENT analysis turbulent intensity for models is a variable input parameter in term of percentage so it can be firstly measured from experiment than provided in the simulation.

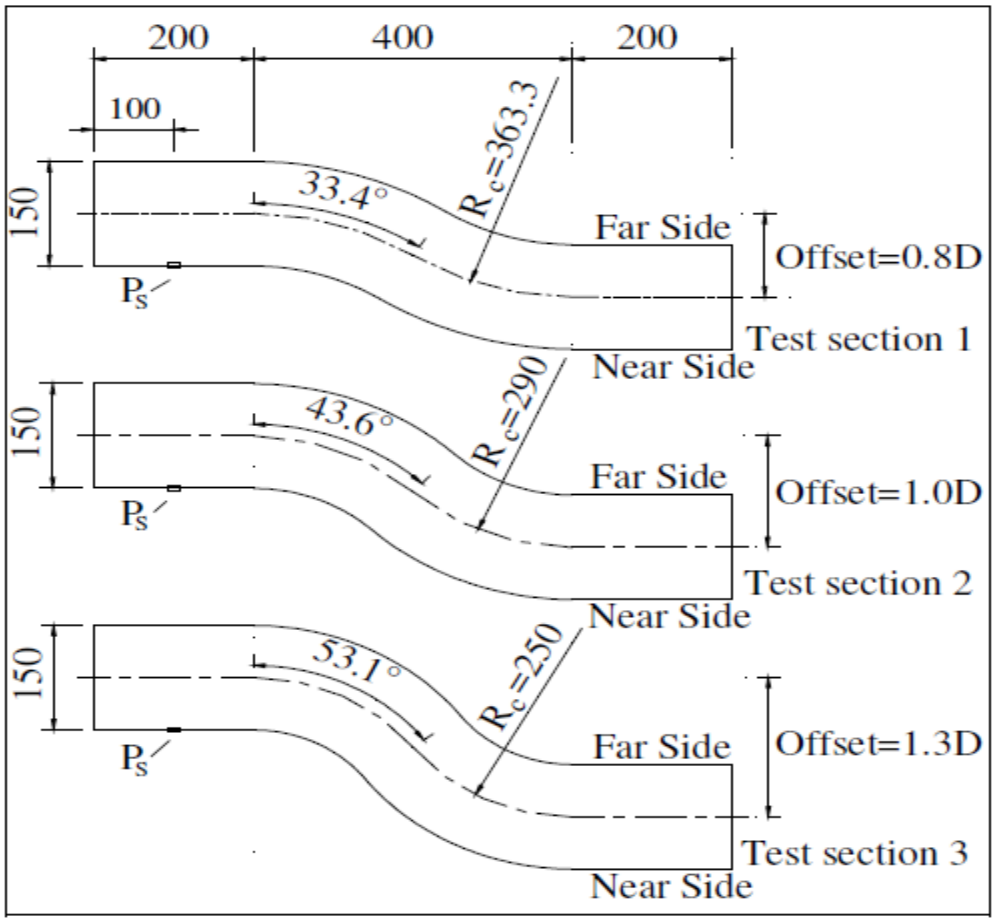

REFERENCES

[1] Anderson, B.H., and Gibb, J., Vortex-Generator Installation Studies on Steady-State and Dynamic Distortion, Journal of Aircraft, Vol. 35(4) Jul-Aug (1998), pp. 513-520.

[2] Anderson, B.H., Reddy, D.R. and Kapoor, K., Study on Computing Separating Flows Within a Diffusing Inlet S-duct, Journal of Propulsion and Power, Vol. 10(5) (1994), pp. 661-667.

[3] Anderson, B.H., Taylor, A.M.K.P., Whitelaw, J.H. and Yianneskis, M., 1982. Developing Flow in S shaped Ducts. In: Proceeding of Second Symposium on the Application of LDA to Fluid Mechanics, Lisbon, Portugal, Paper 4.2, 17 p.

[4] Bansod, P., and Bradshaw, P., The Flow in S-Shaped Ducts, Aeronautical Quarterly, Vol. 23 (1972), pp. 131-140.

[5] Cheng, K.C. and Shi, L. Visualizations of Developing Secondary Flow and Measurements of Velocity Profiles in a Curved Square Duct with and without an Offset Bend. In: Flucome '91, 3rd Triennial International Symposium on Fluid Control, Measurement, and Visualization, San Francisco, USA, (1991) pp. 415-422.

[6] Gad-el Hak, M. and Bushnell, D.M., Separation Control: Review, Transactions of ASME: Journal of Fluid Engineering, Vol. 113(1) Mar (1991), pp 5-30.

[7] Guo R.W. and Seddon J., 1983. The Swirl in an S-duct of Typical Air Intake Proportions, Aeronautical Quarterly, 34(2) 99-129.

[8] Kitchen, B.J. and Bowyer, J.M. Jr., Towards the Optimization of a Non-diffusing Two Dimensional, S-shaped Duct, In: Forum of Turbulent Flows, ASME Fluid Engineering Division FED, San Diego, USA, Vol. 76 (1989), pp 85-92.

[9] M. Norouzia, M.H. Kayhani, C.Shu, M.R.H. Nobari et al. (2010), Flow of second-order fluid in a curved duct with square cross-section, J. Non-Newtonian Fluid Mech.165 (2010) 323–339.

[10] Rojars, J., Whitelaw, J.H. and Yianneskis, M., Developing Flows in S-shaped Diffusers Part I: Square to Rectangular Cross Section Diffuser, NASA Contractor Report 3631, (1983), 50 p.

[11] Sullerey, R.K., and Pradeep, A.M., Effectiveness of Flow Control Devices on S-Duct Diffuser Performance in the Presence of Inflow Distortion, International Journal of Turbo and Jet-Engines, Vol. 19(4) (2002), pp. 259-270.

[12] Taylor A.M.K.P., Whitelaw J.H. and Yianneskis M., 1984. Developing Flow in S-shaped Ducts 2: Circular Cross-section Duct, NASA Contractor Report 3759, 60 p.

[13] Thye, N. Y., 2009.A Thesis, Doctor of Philosophy, National University of Singapore.

[14] Tilak T. Chandratilleke, NimaNadim, Ramesh Narayanaswamy et al (2012) Vortex structure-based analysis of laminar flow behavior and thermal characteristics in curved ducts, International Journal of Thermal Sciences 59 (2012) 75e86.

[15] Whitelaw, J.H. and Yu, S.C.M., 1993a. Turbulent Flow Characteristics in an S-shaped Diffusing Duct, Flow Measurement and Instrumentation, 4(3)171-179.

[16] Whitelaw, J.H. and Yu, S.C.M., 1993b. Velocity Measurements in an S-shaped Diffusing Duct, Experiments in Fluids, 15(3-4) 364-367.

[17] Xiaoyun Wu, Sangding Lai, Kyoji Yamamoto, Shinichiro Yanase et al (2011), Vortex Patterns of the Flow in a Curved Duct, ICSGCE 2011: 27–30 September 2011, Chengdu, China

[18] Yu, S.C.M. and Goldsmith, E.L., 1994. Some Aspects of the Flow in S-shaped Diffusing Ducts, Aeronautical Journal, 98(978)305-310.